IMMUNOLOGY

The activation of the adaptor protein STING depends on its interactions with the phospholipid PI4P

Rutger D. Luteijn[1]*, Sypke R. van Terwisga[1], Jill E. Ver Eecke[1], Liberty Onia[2], Shivam A. Zaver[3], Joshua J. Woodward[3], Richard W. Wubbolts[4], David H. Raulet[2]*†, Frank J. M. van Kuppeveld[1]†

Copyright © 2024 The Authors, some rights reserved; exclusive licensee American Association for the Advancement of Science. No claim to original U.S. Government Works

Activation of the endoplasmic reticulum (ER)–resident adaptor protein STING, a component of a cytosolic DNA–sensing pathway, induces the transcription of genes encoding type I interferons (IFNs) and other proinflammatory factors. Because STING is activated at the Golgi apparatus, control of the localization and activation of STING is important in stimulating antiviral and antitumor immune responses. Through a genome-wide CRISPR interference screen, we found that STING activation required the Golgi-resident protein ACBD3, which promotes the generation of phosphatidylinositol 4-phosphate (PI4P) at the trans-Golgi network, as well as other PI4P-associated proteins. Appropriate localization and activation of STING at the Golgi apparatus required ACBD3 and the PI4P-generating kinase PI4KB. In contrast, STING activation was enhanced when the lipid-shuttling protein OSBP, which removes PI4P from the Golgi apparatus, was inhibited by the US Food and Drug Administration–approved antifungal itraconazole. The increase in the abundance of STING-activating phospholipids at the trans-Golgi network resulted in the increased production of IFN-β and other cytokines in THP-1 cells. Furthermore, a mutant STING that could not bind to PI4P failed to traffic from the ER to the Golgi apparatus in response to a STING agonist, whereas forced relocalization of STING to PI4P-enriched areas elicited STING activation in the absence of stimulation with a STING agonist. Thus, PI4P is critical for STING activation, and manipulating PI4P abundance may therapeutically modulate STING-dependent immune responses.

Downloaded from https://www.science.org on March 18, 2024

INTRODUCTION

Cytosolic DNA is a key danger signal that can be detected by various cytosolic DNA-sensing pathways, most notably the cGAS/STING pathway. Upon activation, this innate immune pathway promotes the expression of inflammatory molecules, including type I interferons (IFNs), cytokines, and chemokines, and is thereby critical for shaping the innate and adaptive immune response. The cGAS/STING pathway senses cytosolic DNA originating from viruses and bacteria (*1*) as well as cyclic dinucleotides (CDNs) produced by certain bacteria (*2*–*4*). The STING pathway is also activated by cytosolic self-DNA, which accumulates in cells in certain autoinflammatory disorders (*5*, *6*), and in cells subjected to DNA damage, as occurs in premalignant and tumor cells (*7*, *8*). In addition, the cGAS/STING pathway plays a role in the immune response to certain RNA viruses, such as dengue virus (*9*), influenza virus (*10*), and coronaviruses (*11*). RNA viruses may trigger the cGAS/STING pathway by stimulating the accumulation of host DNA in the cytosol of infected cells (*12*). Moreover, STING can be activated by virus-induced lipid membrane remodeling events (*10*). The critical role of STING in the immune response to virus infection is underlined by the observation that numerous viruses—including herpes virus, vaccinia virus, dengue virus and SARS-coronavirus (*11*)—counteract STING activation, thereby evading the host immune response.

STING regulation is a complex process that starts with binding of endoplasmic reticulum (ER)–localized STING to its ligands, most notably CDNs. The mammalian CDN 2′3′- cyclic-di-GMP-AMP (2′3′-cGAMP) is produced endogenously by the enzyme cGAS upon detection of cytosolic DNA and binds STING with nanomolar affinity. In addition, 2′3′-cGAMP can be imported from the extracellular environment or neighboring cells to activate STING (*13*). Similarly, synthetic phosphodiesterase-resistant CDNs, such as 2′3′-RR cyclic-di-AMP (CDA) (RR CDA) used in cancer immunotherapy, are transported into the cell and bind ER-localized STING with high affinity (nanomolar range) (*14*). Upon CDN binding, STING translocates to the Golgi compartment by a poorly understood process that is dependent on an increase in the production of the phospholipid phosphatidylinositol 3-phosphate at the ER (*15*). At the trans-Golgi network (TGN), STING oligomers are phosphorylated by TBK1, and STING subsequently activates the transcription factors interferon regulatory factor 3 (IRF3) and nuclear factor κB (NF-κB). To prevent sustained immune activation, activated STING is degraded in the endolysosomal compartment (*13*).

Anomalies at any of these steps can lead to aberrant STING activation, resulting in auto inflammatory conditions (*16*), or diminished STING signaling and immune escape, as observed in certain tumors and virus-infected cells (*17*, *18*). Furthermore, STING activity can be redirected to generate a tumor- or virus-promoting environment (*19*, *20*). Many of the factors orchestrating the quality and intensity of the STING response remain unknown.

To find factors regulating STING activity, we previously performed a genome-wide CRISPR interference (CRISPRi) screen (*21*). Using this method, we successfully identified a transporter that imports STING agonists from the extracellular environment. In addition, we identified many host factors that may drive or dampen STING activation. One of the top hits in this screen that was necessary for strong activation of the STING pathway was the gene encoding ACBD3. This

[1]Virology Section, Infectious Diseases and Immunology Division, Department of Biomolecular Health Sciences, Faculty of Veterinary Medicine, Utrecht University, Utrecht, Netherlands. [2]Department of Molecular and Cell Biology, and Cancer Research Laboratory, Division of Immunology and Molecular Medicine, University of California, Berkeley, CA, USA. [3]Department of Microbiology, University of Washington, Seattle, WA, USA. [4]Centre for Cell Imaging, Division of Cell Biology, Metabolism and Cancer, Department of Biomolecular Health Sciences, Faculty of Veterinary Medicine, Utrecht University, Utrecht, Netherlands.
*Corresponding author. Email: raulet@berkeley.edu (D.H.R); r.d.luteijn@uu.nl (R.D.L.)
†These authors contributed equally to this work.

Golgi-resident protein is a multifunctional protein that promotes the distribution of phosphatidylinositol 4-phosphate (PI4P) to the Golgi by recruiting the PI4P kinase PI4KB (*22*) and has not previously been implicated in STING activation. Here, we showed that ACBD3 increased STING activation by promoting STING mobilization to the Golgi. We further showed that STING signaling depends on other components that regulate PI4P levels or localization, including Sac1, PI4KB, and the PI4P-cholesterol exchanger OSBP, underscoring the importance of PI4P in STING signaling. The phospholipid PI4P played a role in recruiting several proteins to the Golgi and the function of those proteins (*23*), and our results indicated a role in STING recruitment and/or retention in the Golgi and STING signaling in the Golgi. The role of the PI4P pathway in STING signaling was especially interesting, because it demonstrated the therapeutic potential of modifying the immune response by STING by targeting the pathway with US Food and Drug Administration (FDA)–and European Medicines Agency (EMA)–approved drugs.

RESULTS

ACBD3 expression is necessary for efficient STING activation

To confirm the role of ACBD3 in STING activation, we depleted the expression of *ACBD3* in THP-1 monocytes using CRISPRi guide RNAs (gRNAs) (fig. S1A). To measure STING activation in these cells, we expressed an ISRE-IFNb-tdTomato reporter, which robustly induces tdTomato expression in response to STING activation (*21*). Control cells stimulated with the highly potent STING agonist 2′3′-RR CDA expressed the fluorescent tdTomato reporter, but the reporter response was diminished in cells transduced with gRNAs targeting *ACBD3* or *IRF3*, the latter a STING-activated transcription factor critical for reporter gene expression (Fig. 1, A and B). STING-independent reporter activation by human IFN-β was not affected. Restoration of ACBD3 expression rescued reporter activation in ACBD3-depleted cells (Fig. 1C).

As further confirmation, we generated ACBD3 knockout cells in THP-1 cells using the conventional CRISPR-Cas9 system (fig. S1B). Two distinct knockout clones lacking *ACBD3* expression showed highly reduced reporter activation to a variety of STING agonists, including 2′3′-cGAMP, 2′3′-RR-CDA, the bacterial CDNs 3′3′-cGAMP and 3′3′-CDA, and the non-CDN STING agonist diABZI (Fig. 1D). Similarly, *ACBD3* knockout 293T cells [transduced to express enhanced green fluorescent protein (eGFP)–mouse STING (eGFP-mSTING)] had reduced reporter activation upon STING activation (fig. S2, A and B). STING activation leads to downstream transcription of inflammatory genes, including *IL-6*, *CXCL10*, and *IFNB1*. *ACBD3* knockdown and knockout THP-1 cells were defective for expression of all of these genes after stimulation with STING agonist (Fig. 1, E to G).

ACBD3 is important for STING phosphorylation, clustering, and relocalization

To further investigate the role of ACBD3 in STING activation, we determined the effects of ACBD3 depletion on the different processes involved in STING activation. The uptake of 2′3′-cGAMP or 3′3′-CDA from the extracellular environment was not affected in cells lacking ACBD3, in contrast with cells lacking SLC19A1, one of the CDN transporters (Fig. 2A). A second critical step in immune activation by STING is STING phosphorylation at S366, which is required for downstream activation of IRF3. Upon depletion of ACBD3, STING phosphorylation in response to stimulation with 2′3-RR CDA was strongly reduced (Fig. 2B), whereas depletion of the downstream transcription factor IRF3 had no effect on STING phosphorylation. As expected, depletion of the SLC19A1 transporter also diminished STING phosphorylation.

STING phosphorylation requires STING trafficking from the ER to the TGN, where STING palmitoylation promotes the formation of activation clusters needed for downstream signaling (*24*). STING is recruited to perinuclear clusters in HA-STING–expressing 293T cells and THP-1 cells upon STING activation (Fig. 2C and fig. S3). These clusters colocalized with the Golgi-resident protein ACBD3. Depletion of *ACBD3* expression prevented STING clustering in cells stimulated with 2′3′-RR-CDA. Instead, STING localization was similar to that in unstimulated cells, presumably in the ER. Similarly, live-cell imaging of eGFP-tagged mouse STING (eGFP-mSTING) showed cluster formation in the Golgi region in control 293T cells but not in knockout cells lacking *ACBD3* (Fig. 2, D and E). Thus, ACBD3 is required for the relocalization of STING upon activation.

STING localizes to PI4P-rich environments

ACBD3 binds and recruits PI4KB to the TGN (*25*). In line with this, ACBD3 colocalized to TGN46 (a Golgi marker) and PI4KB-enriched perinuclear clusters in unstimulated THP-1 cells (Fig. 3, A and B). In ACBD3-depleted THP-1 cells, perinuclear PI4KB clusters were absent (Fig. 3B). Similarly, PI4KB coclustered with PI4P in control cells, whereas perinuclear clustering of PI4P and PI4KB was lost in ACBD3-depleted cells (Fig. 3C). PI4P and p-STING colocalized in perinuclear clusters upon STING activation in control cells but not in ACBD3-depleted cells (Fig. 3D).

PI4KB and OSBP inhibition have opposite effects on STING activation

The role of PI4KB in STING activation was supported by our genome-wide screens for STING-associated factors, where PI4KB was identified in the screen for genes whose depletion resulted in weaker activation of the pathway (*21*). We confirmed the role of PI4KB in STING pathway activation by treating cells with the PI4KB inhibitor BF738735 (*26*), which reduced STING pathway activation (Fig. 4A). Furthermore, when we depleted PI4KB expression using CRISPRi gRNAs, we observed that gRNAs that depleted progressively more *Pi4kb* mRNA led to greater deficiency in reporter activation after stimulation with STING agonist (Fig. 4, B and C).

Upon shuttling to the ER, PI4P is ultimately hydrolyzed by the phosphatase Sac1. Overexpression of wild-type Sac1 (Sac1-WT) or a Sac1-K583A K585A double mutant that localizes to the TGN (Sac1-KKAA) effectively depletes PI4P at the TGN, in contrast to a phosphatase-dead version of Sac1 (*27*). In 293T cells expressing eGFP-mSTING, overexpression of Sac1-WT or the Sac1-KKAA mutant significantly impaired STING activation by CDNs compared with overexpression of the phosphatase-dead mutant of Sac1 (Fig. 4D). Together, these results suggest that PI4P levels at the TGN are important for proper STING trafficking and activation.

Another protein that affects PI4P levels at the TGN is oxysterol binding protein (OSBP). This protein is localized at membrane contact sites between the TGN and the ER by interacting with VAP at the ER and PI4P at the TGN (*28*). OSBP shuttles PI4P from the TGN to the ER and/or to lysosomes in exchange for cholesterol. Inhibition of OSBP by the plant-extract OSW-1 or the FDA-approved drug itraconazole results in the accumulation of PI4P at the TGN (*29*, *30*). In

Downloaded from https://www.science.org on March 18, 2024

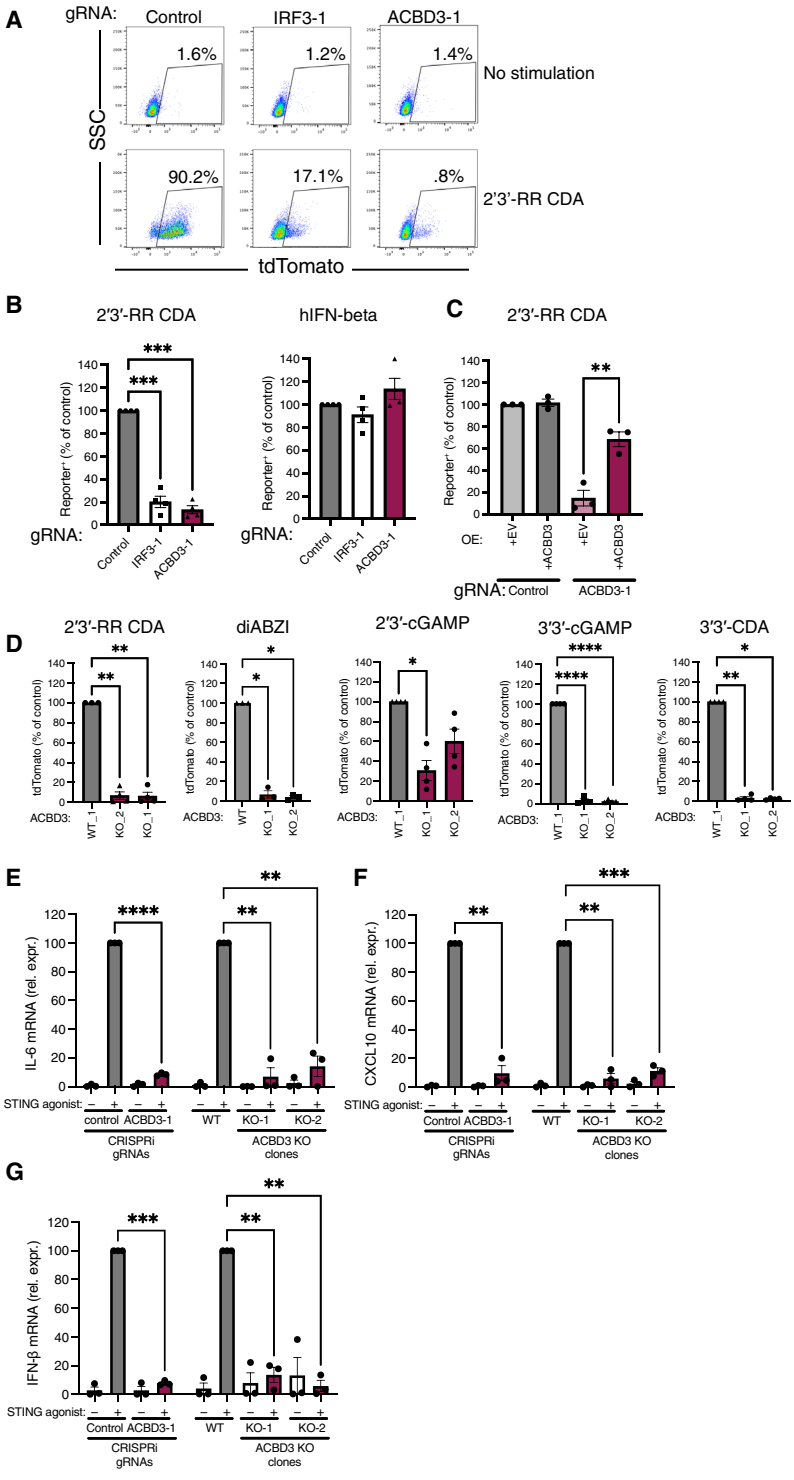

Fig. 1. ACBD3 expression is necessary for tdTomato reporter activation and cytokine production induced by STING agonists. (**A**) dCas9-KRAB–expressing THP-1 cells transduced with nontargeting gRNA (control), IRF-3–targeting gRNA (IRF3-1), or ACBD3-targeting gRNA (ACBD3-1) were exposed to 2′3′-RR CDA, and tdTomato expression was analyzed by flow cytometry. Representative dot plots of $n = 3$ biological replicates of three independent experiments are shown. (**B**) THP-1 cells expressing the indicated CRISPRi gRNAs or nontargeting gRNA (control) were stimulated with 2′3′-RR CDA or human IFN-β, and tdTomato expression was quantified as in (A). (**C**) Control THP-1 cells and THP-1 cells expressing ACBD3-1 CRISPRi gRNA transduced with ACBD3 or empty vector (EV) were stimulated with 2′3′-RR CDA analyzed as in (A). (**D**) THP-1 control clone (WT1) or two THP-1 clones lacking ACBD3 were stimulated with the indicated STING agonists and analyzed as in (A). (**E** to **G**) *IL-6* (E), *CXCL10* (F), or *IFNB1* (G) mRNA levels in THP-1 cells expressing control or ACBD3 CRISPRi gRNAs or THP-1 WT or ACBD3 KO clones stimulated with 2′3′-RR CDA (RR-CDA). (B to G) Means ± SEM of at least $n = 3$ biological replicates of three independent experiments are shown. (B and D) Statistical tests were performed on unnormalized data. We performed paired one-way ANOVA followed by Dunnett's multiple comparisons post tests to compare each treatment group with the control group. $^{*}P < 0.05$, $^{***}P < 0.001$, and $^{****}P < 0.0001$; ns, not significant. (C) A one-tailed paired *t* test was performed on data that had not been normalized to the control sample. (E to G) To compare each treatment group with the normalized control value (set at 100), we performed one-sample *t* tests. $^{*}P < 0.05$, $^{**}P < 0.01$, $^{***}P < 0.001$, and $^{****}P < 0.0001$.

light of our finding that STING activation was impaired when PI4P levels were reduced as a result of targeting ACBD3 or PI4KB, we hypothesized that increasing PI4P concentrations at the TGN by targeting or inhibiting OSBP might result in enhanced STING signaling. We tested this by combining limiting doses of RR-CDA or 2′3′-cGAMP, which induced only small responses in THP-1 cells, with itraconazole or OSW-1, which did not, by themselves, activate the STING pathway. Combining the OSBP inhibitors with limiting doses of STING agonist resulted in a marked increase in reporter activation (Fig. 4, E and F, and fig. S4A). Synergistic pathway activation was also observed when we tested induction of the endogenous transcripts *CXCL10* and *IFNB1* (Fig. 4G and fig. S4B) or IFN-β1 protein

Downloaded from https://www.science.org on March 18, 2024

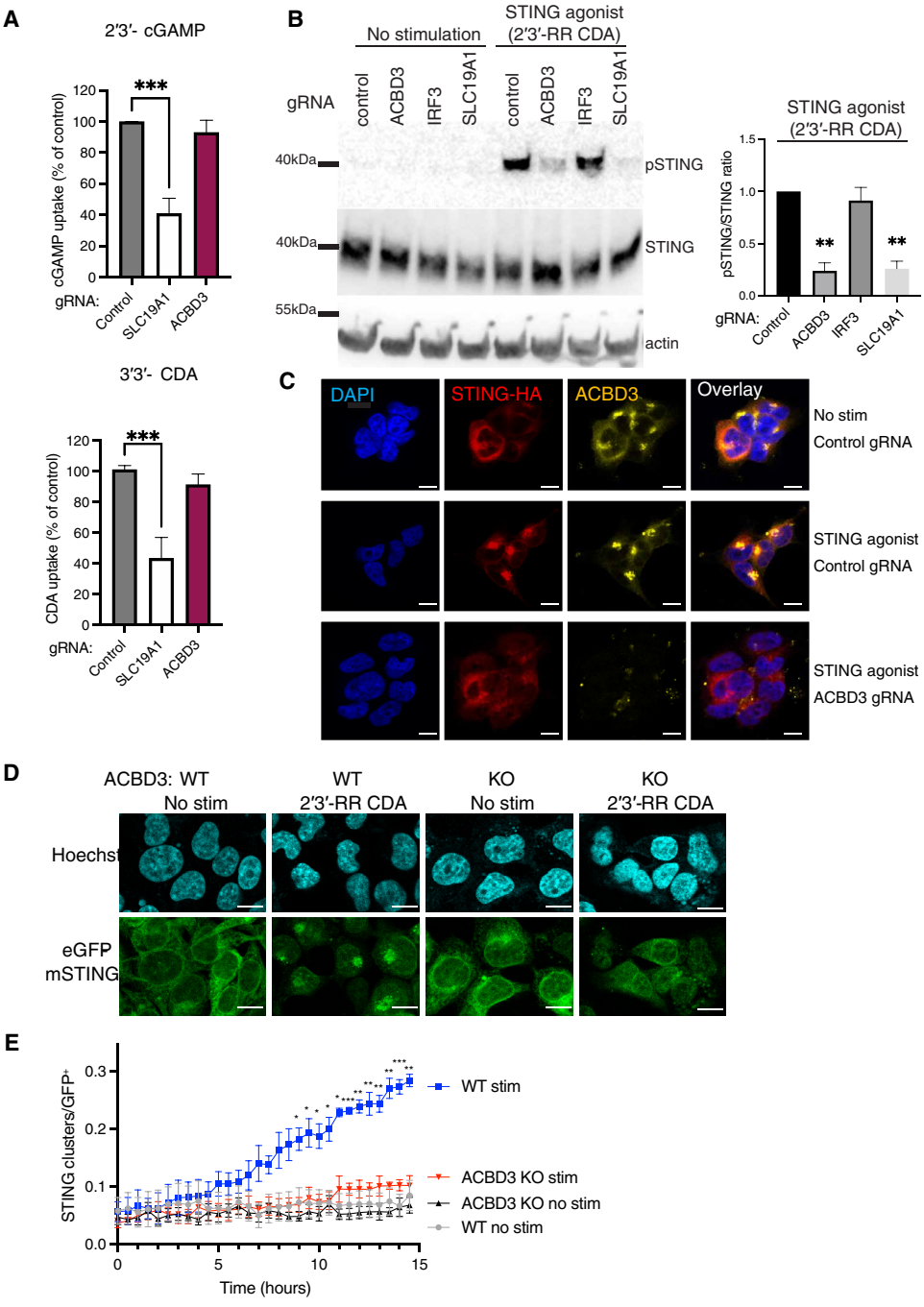

Fig. 2. ACBD3 is important for STING phosphorylation, clustering, and relocalization. (**A**) Normalized [^{32}P]2′3′-cGAMP (cGAMP) and [^{32}P]3′3′-c-di-AMP (CDA) uptake by THP-1 monocytes transduced with a nontargeting control CRISPRi gRNA or SLC19A1 or ACBD3 CRISPRi gRNA. Means ± SEM of $n = 3$ biological replicates of three independent experiments are shown. To compare each treatment group with the normalized control value (set at 100), we performed one-sample *t* tests. ***$P < 0.001$. (**B**) Immunoblot analysis of protein expression and phosphorylation in THP-1 cells expressing indicated CRISPRi gRNAs. Cells were stimulated for with 2′3′-RR CDA or left unstimulated. p-STING, STING phosphorylated on S366. Representative images of $n = 3$ biological replicates of three independent experiments are shown. Bars show the relative ratios of pSTING over total STING expression in 2′3′-RR CDA-treated samples. Means ± SEM of $n = 3$ biological replicates of three independent experiments are shown. To compare each treatment group with the normalized control value (set at 1), we performed one-sample *t* tests. **$P < 0.01$. (**C**) Immunofluorescence of 293T cells stably transduced with STING-HA and a control CRISPRi gRNA or an ACBD3-targeting CRISPRi gRNA. Cells were stimulated with 2′3′-RR CDA (STING agonist) and stained for HA or ACBD3. Representative images of $n = 3$ biological replicates of three independent experiments are shown. Scale bars, 10 μm. (**D**) Immunofluorescence live-cell imaging of eGFP-tagged mouse-STING stably transduced in control 293T cells or 293T cells lacking ACBD3 [knockout (KO)] stimulated with 2′3-RR CDA. Representative images of $n = 4$ biological replicates of four independent experiments are shown. Scale bars, 10 μm. (**E**) Number of STING clusters/eGFP$^+$ cells shown in (D) was quantified over time using the "particle analysis" function of ImageJ. Means ± SEM of $n = 4$ biological replicates of four independent experiments are shown. We performed two-way ANOVA followed by Tukey's multiple comparisons test to compare stimulated WT and stimulated ACBD3 KO treatment groups. *$P < 0.05$, **$P < 0.01$, and ***$P < 0.001$.

secretion (fig. S4C). The effect was dependent on STING expression (fig. S4D). Last, immune activation triggered by transfection of double-stranded DNA (dsDNA), which induces endogenous production of 2′3′-cGAMP, was also enhanced in the presence of itraconazole (fig. S4E).

We investigated the role of PI4KB in STING activation by OSBP inhibitors using the PI4KB inhibitor BF738735. PI4KB inhibition completely reverted the amplifying effect of itraconazole on STING activation (Fig. 4H), thereby indicating that OSBP inhibition promotes STING activation via PI4P.

In addition to chemical inhibition of OSBP, we targeted OSBP functionally by expressing IFN-inducible transmembrane protein 3 (IFITM3) in 293T cells. IFITM3 disrupts the interaction between OSBP and VAP at membrane contact sites, thereby preventing OSBP-mediated cholesterol-PI4P exchange (*29*, *31*). Expression of FLAG-tagged IFITM3 did not promote STING phosphorylation under resting conditions but significantly promoted STING activation upon stimulation with 2′3′-cGAMP (fig. S4F). Overall, these results indicate that agents modulating PI4P levels may have promise for either boosting or restraining STING pathway activation.

Downloaded from https://www.science.org on March 18, 2024

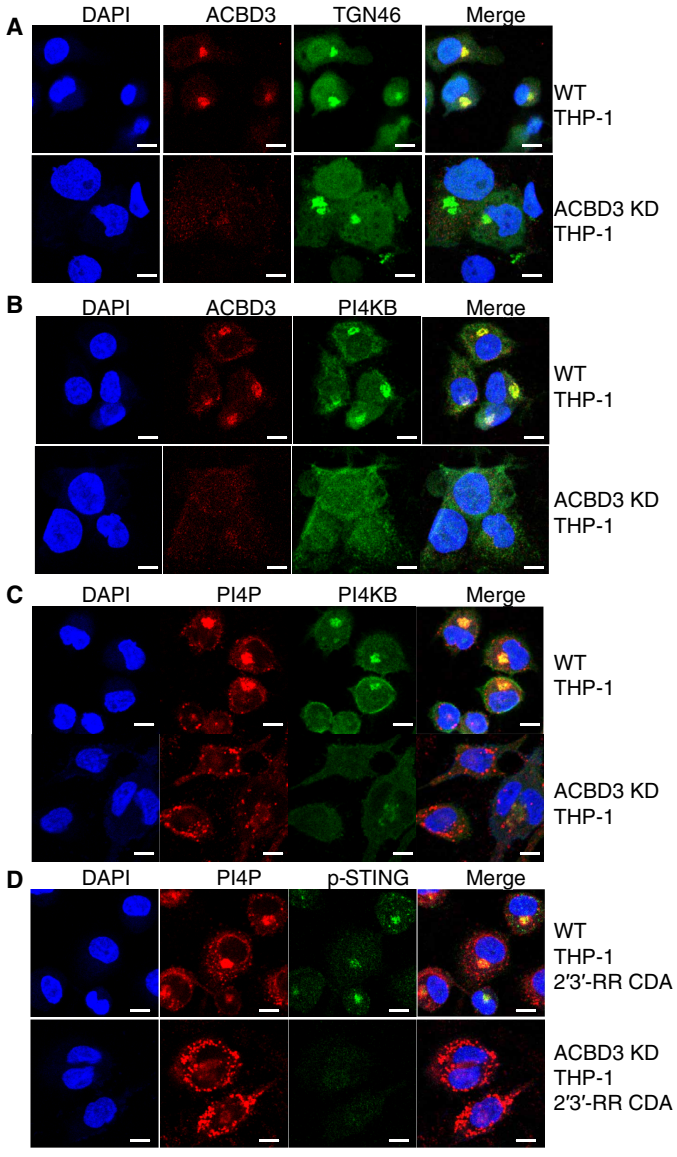

Fig. 3. STING localizes to PI4P-rich environments. (**A** to **D**) Immunofluorescence images of THP-1 cells expressing control or ACBD3 CRISPRi gRNAs stained for the indicated proteins. During cell culturing, THP-1 cells were treated with PMA to make them adherent to the coverslips. In (D), THP-1 cells were stimulated with 2′3′-RR CDA before staining. Scale bars, 10 μm. Representative images of at least $n = 3$ biological replicates of three independent experiments are shown.

OSBP inhibition increases STING activation and decreases STING degradation

To further dissect the mechanism by which OSBP inhibition increases STING activation, we tested the phosphorylation status of STING at different time points after stimulation (Fig. 5A). Relative to the results after stimulation with 2′3′-cGAMP alone, the addition of itraconazole or OSW1 resulted in an increase in STING phosphorylation at 8 hours (Fig. 5, A and B; see Fig. 5B for quantification). OSBP inhibition in the absence of STING agonists did not promote STING phosphorylation (fig. S5A). When combined with 2′3′-cGAMP, OSBP inhibitors also enhanced the phosphorylation of TBK-1 and IRF3 and the degradation of IκBα, the latter a hallmark of NF-κB activation (Fig. 5B). Furthermore, stimulating cells with limiting amounts of 2′3′-cGAMP in the presence of OSBP inhibitors promoted eGFP-mSTING clustering (Fig. 5, C and D). The pronounced STING activation induced by itraconazole did not result from an increase in 2′3′-cGAMP taken up from the extracellular environment (fig. S5B).

After activation, STING traffics to the endolysosomal compartment for degradation (*32*). To quantify STING degradation, eGFP-mSTING expression was measured 20 hours after activation in the presence of dimethyl sulfoxide (DMSO) or itraconazole (Fig. 5E). Upon activation, eGFP-mSTING was degraded in control cells, but degradation was significantly reduced in the presence of itraconazole (Fig. 5F).

Mutating the PI4P binding site of STING prevents STING activation

To understand how PI4P affects STING activation and localization, we performed a number of complementary experiments. First, we expressed a STING mutant incapable of binding PI4P because of the replacement of four positively charged amino acids in the α3 helix of STING with glutamate residues (STING 4POSE) (*33*). In contrast to WT STING, the STING 4POSE mutant showed no phosphorylation upon stimulation with 2′3-RR CDA (Fig. 6A). Furthermore, upon stimulation, the PI4P-binding mutant did not form activation clusters over time (Fig. 6B).

Second, we made use of the natural V155M mutation in human STING (V154M in mouse STING), which causes constitutive STING activation and localization at the Golgi (*34*), by mimicking a ligand-bound conformation of STING (*35*). In line with this, mouse STING V154M expressed in 293T cells formed clusters (Fig. 6C) and was phosphorylated in the absence of stimulation (Fig. 6D). Introduction of the V154M mutation in the STING 4POSE variant prevented constitutive STING clustering and phosphorylation. These results suggest that PI4P binding by STING is essential for activation of WT STING and constitutive STING activation by the V154M variant.

Targeting STING to PI4P-enriched environments promotes STING activation

Last, we asked whether forced relocalization of WT STING to a PI4P-enriched environment would cause STING activation, even in the absence of STING agonist stimulation. To accomplish this, we targeted eGFP-STING to a PI4P-enriched environment using a Camelidae-derived nanobody specific for GFP (*36*). This GFP-binding protein (GBP) was fused to the monomeric red fluorescent protein mScarlet-I (*37*) to monitor expression and colocalization with eGFP-STING. mScarlet-GBP colocalized with eGFP-STING and formed clusters upon stimulation with STING agonists, unlike mScarlet lacking a GBP domain (fig. S6A). Next, we fused mScarlet-GBP to the pleckstrin homology (PH) domain of FAPP1, which is a well-defined PI4P sensor (*38*). Coexpression of mScarlet-GBP-FAPP1 and eGFP-STING markedly promoted STING clustering (Fig. 7A and fig. S6A). FAPP1 and STING coclusters colocalized in PI4P-enriched domains (fig. S6B). These PI4P-enriched clusters contained high levels of phosphorylated STING (Fig. 7A), suggesting robust activation even in the absence of stimulation. Quantification of STING phosphorylation by flow cytometry confirmed significant STING activation in the

Downloaded from https://www.science.org on March 18, 2024

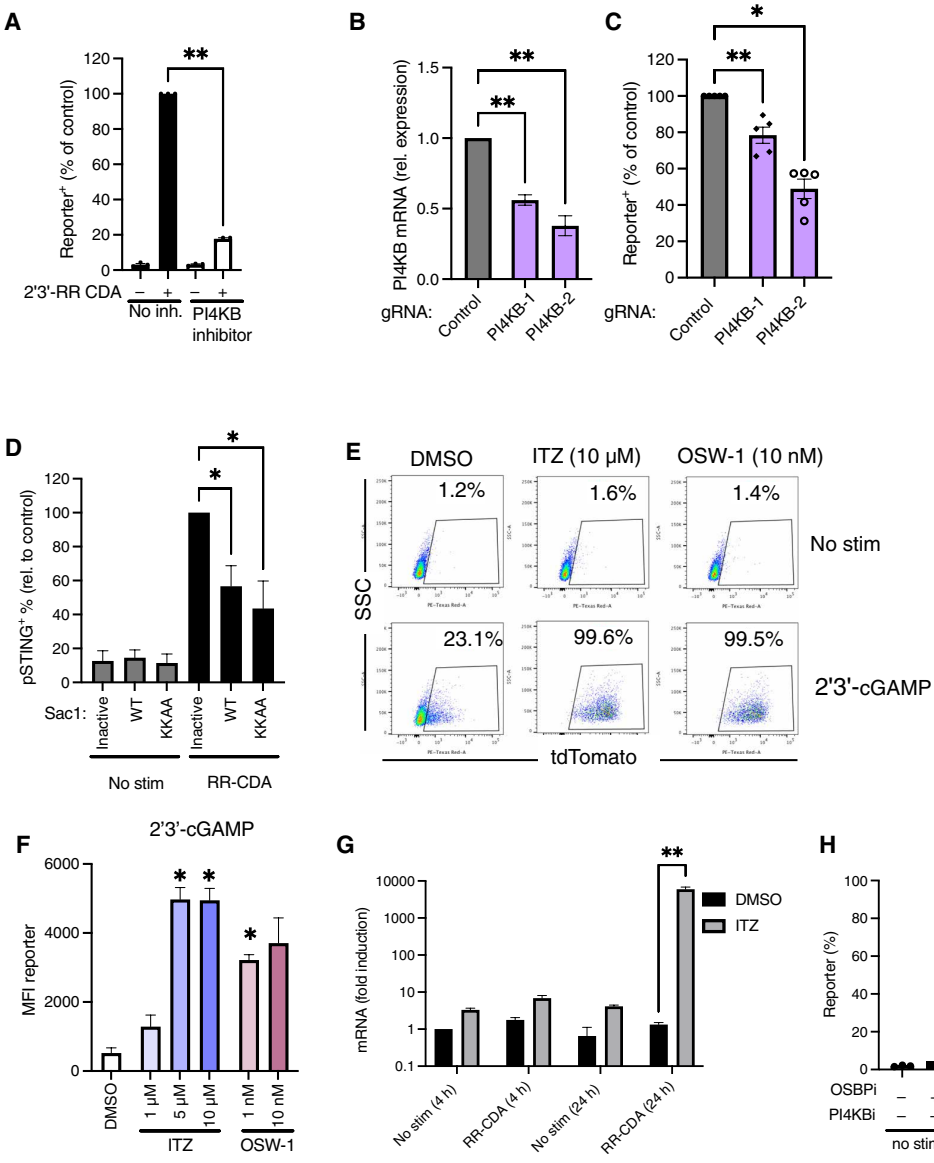

Fig. 4. PI4KB and OSBP inhibition have opposite effects on STING activation. (**A**) THP-1 cells were pre-incubated with the PI4KB inhibitor BF738735 and subsequently stimulated with the STING agonist 2′3′-RR CDA, and tdTomato-reporter expression was quantified by flow cytometry. Means ± SEM of $n = 3$ biological replicates of three independent experiments are shown. A paired one-tailed *t* test was performed on data that were not normalized to the controls. (**B**) *PI4KB* mRNA expression levels in THP-1 cells expressing a control gRNA or gRNAs targeting PI4KB. Means ± SEM of $n = 4$ biological replicates of four independent experiments are shown. One-sample *t* tests were performed to compare each group with the normalized control value set at 1. (**C**) Cells in (B) were stimulated with 2′3′-RR CDA, and tdTomato reporter expression was quantified by flow cytometry. Means ± SEM of $n = 5$ biological replicates of five independent experiments are shown. Statistical tests were performed on unnormalized data. We performed paired one-way ANOVA followed by Dunnett's multiple comparisons post-tests to compare each treatment group with the control group. (**D**) 293T cells expressing eGFP-mSTING were transfected with a phosphatase-dead Sac1 (inactive), active Sac1-WT, or Sac1-KKAA mutant and stimulated or not with 2′3′-RR CDA (RR-CDA). After stimulation, cells were stained for phospho-STING and analyzed by flow cytometry. Means ± SEM of $n = 4$ biological replicates of four independent experiments are shown. One-sample *t* tests were performed to compare each group with the normalized control value set at 100. (**E**) THP-1 cells were preincubated with DMSO or the OSBP inhibitors itraconazole (ITZ) or OSW-1 and stimulated with a limiting concentration of 2′3′-cGAMP or left untreated. Reporter expression was quantified by flow cytometry. Representative images of $n = 3$ biological replicates of three independent experiments are shown. (**F**) Mean fluorescence intensity of tdTomato reporter in THP-1 cells stimulated with a limiting concentration of 2′3′-cGAMP in the presence of DMSO, itraconazole, or OSW-1. Means ± SEM of $n = 3$ biological replicates of three independent experiments are shown. Statistical tests were performed on unnormalized data. We performed paired one-way ANOVA followed by Dunnett's multiple comparisons post-tests to compare each treatment group with the control group. (**G**) *CXCL10* mRNA levels in THP-1 cells pretreated with DMSO or itraconazole and stimulated with a limiting concentration of 2′3′-RR CDA (RR-CDA). Means ± SEM of $n = 3$ biological replicates of three independent experiments are shown. A paired one-tailed *t* test was used to compare the itraconazole group with the DMSO control group. (**H**) tdTomato reporter expression of THP-1 cells pretreated with the PI4KB inhibitor (PI4KBi) BF738735 followed by pretreatment with itraconazole and stimulation with a limiting concentration of 2′3′-cGAMP. Means ± SEM of $n = 3$ biological replicates of three independent experiments are shown. We performed paired one-way ANOVA followed by Dunnett's multiple comparisons post tests to compare the indicated treatment groups with the control group. $^*P < 0.05$, $^{**}P < 0.01$, and $^{***}P < 0.001$.

Downloaded from https://www.science.org on March 18, 2024

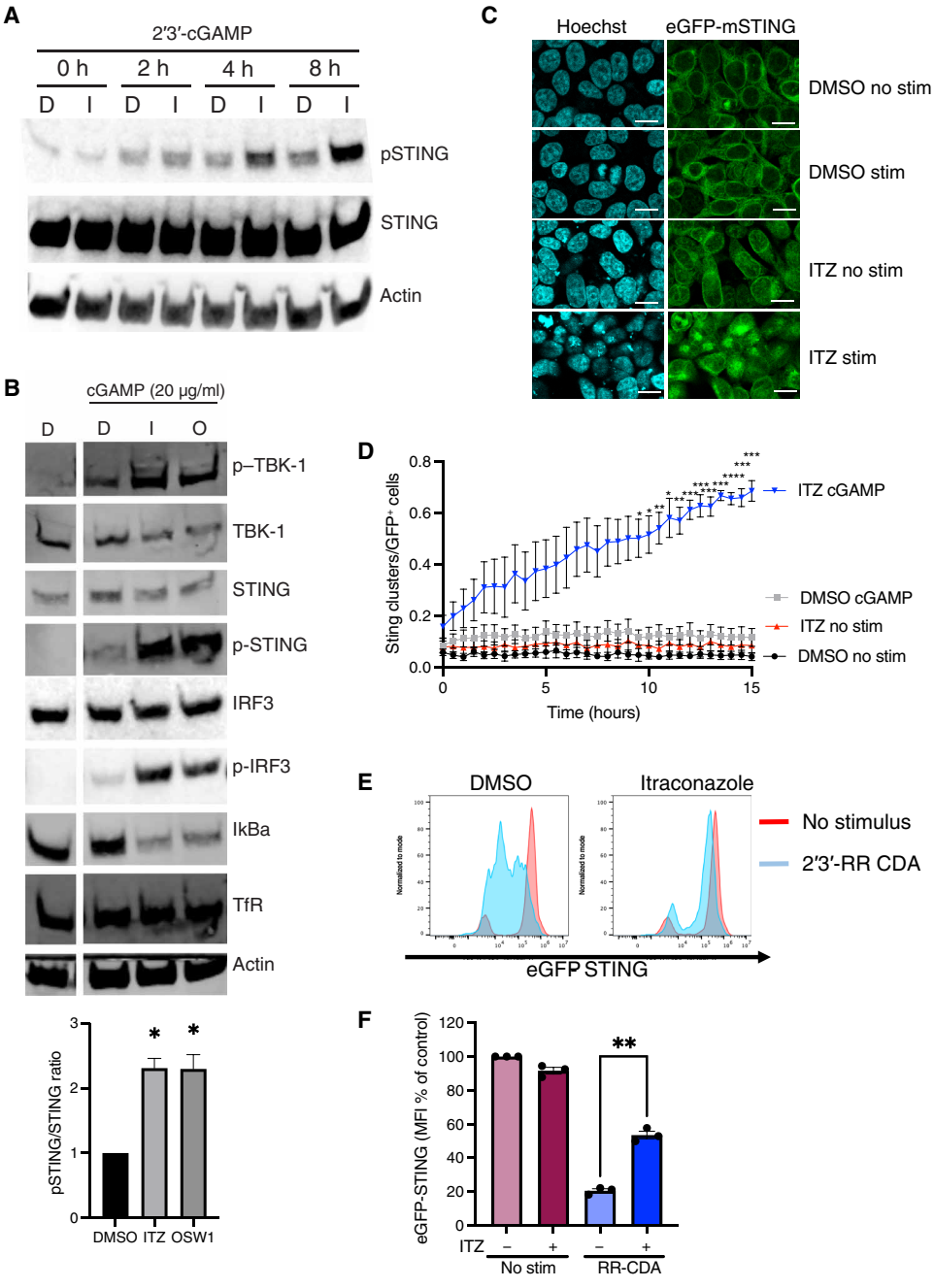

Fig. 5. OSBP inhibition increases STING activation and decreases STING degradation. (**A**) Immunoblot analysis of the indicated (phosphorylated) proteins expressed by THP-1 cells. Cells were pretreated with DMSO (D) or itraconazole (I) and stimulated with 2′3′-cGAMP for the indicated time points. Representative images of $n = 3$ biological replicates of three independent experiments are shown. (**B**) Immunoblot analysis of THP-1 cells pre-incubated as in (A) and stimulated with a limiting concentration of 2′3′-cGAMP for 8 hours. Representative images of $n = 3$ biological replicates of three independent experiments are shown. Bars show the relative ratios of pSTING over total STING expression in 2′3′-cGAMP–treated samples. Means ± SEM of $n = 3$ biological replicates of three independent experiments are shown. To compare each treatment group with the normalized control value (set at 1), we performed one-sample *t* tests. $^{*}P < 0.05$. (**C**) Immunofluorescence live-cell imaging eGFP-tagged mSTING transduced in 293T cells pretreated with DMSO or itraconazole and stimulated with a limiting concentration of 2′3′-cGAMP. Representative images of $n = 4$ biological replicates of four independent experiments are shown. Scale bars, 10 μm. (**D**) The number of STING clusters/GFP^{+} cells shown in (C) was quantified over time using the particle analysis function of ImageJ. Quantification of $n = 4$ biological replicates of four independent experiments is shown. We performed two-way ANOVA followed by Tukey's multiple comparisons test to compare stimulated stimulated ITZ and stimulated DMSO groups. $^{*}P < 0.05$, $^{**}P < 0.01$, $^{***}P < 0.001$, and $^{****}P < 0.0001$. (**E**) Expression of eGFP-tagged mouse STING transduced in THP-1 cells pretreated with DMSO or itraconazole for and stimulated with 2′3′-RR CDA or left unstimulated. Representative image of $n = 3$ biological replicates of three independent experiments is shown. (**F**) Quantification of eGFP-STING in THP-1 cells shown in (E). Means ± SEM of $n = 3$ biological replicates of three independent experiments are shown. A one-tailed paired *t* test was used to compare the indicated groups. $^{**}P < 0.01$.

presence of mScarlet-GBP-FAPP1 but not mScarlet-FAPP1 or mScarlet-GBP (Fig. 7B), Reciprocally, targeting FAPP1-eGFP with mScarlet-GBP-STING also promoted STING clustering (fig. S7A) and significantly increased STING phosphorylation (fig. S7B).

Expression of mScarlet-GBP-FAPP1 also promoted clustering of the eGFP-STING 4POSE mutant defective in PI4P binding (Fig. 7C), but in this mutant, STING phosphorylation was not activated despite relocalization of the mutant STING to PI4P-enriched membranes (Fig. 7D). These results suggest that the interaction between PI4P and STING in PI4P-enriched membranes is essential for STING phosphorylation and activation (Fig. 8).

DISCUSSION

Here, we showed that the phospholipid PI4P plays a critical role in the STING-induced immune response. Upon activation, STING trafficked to PI4P-positive structures that were regulated by PI4KB and ACBD3, the latter being one of the top hits in our screen for genes required for STING activation (*21*). Depleting ACBD3 blocked STING activation by various CDNs and other STING agonists by preventing STING trafficking to the TGN. STING trafficking from the ER to the TGN is critical for downstream immune activation. At the TGN, STING forms oligomers that interact with TBK1 (*39*), leading to phosphorylation of TBK1, STING, and IRF3 (*13*). After immune activation, STING is degraded by the endolysosomal system or

Downloaded from https://www.science.org on March 18, 2024

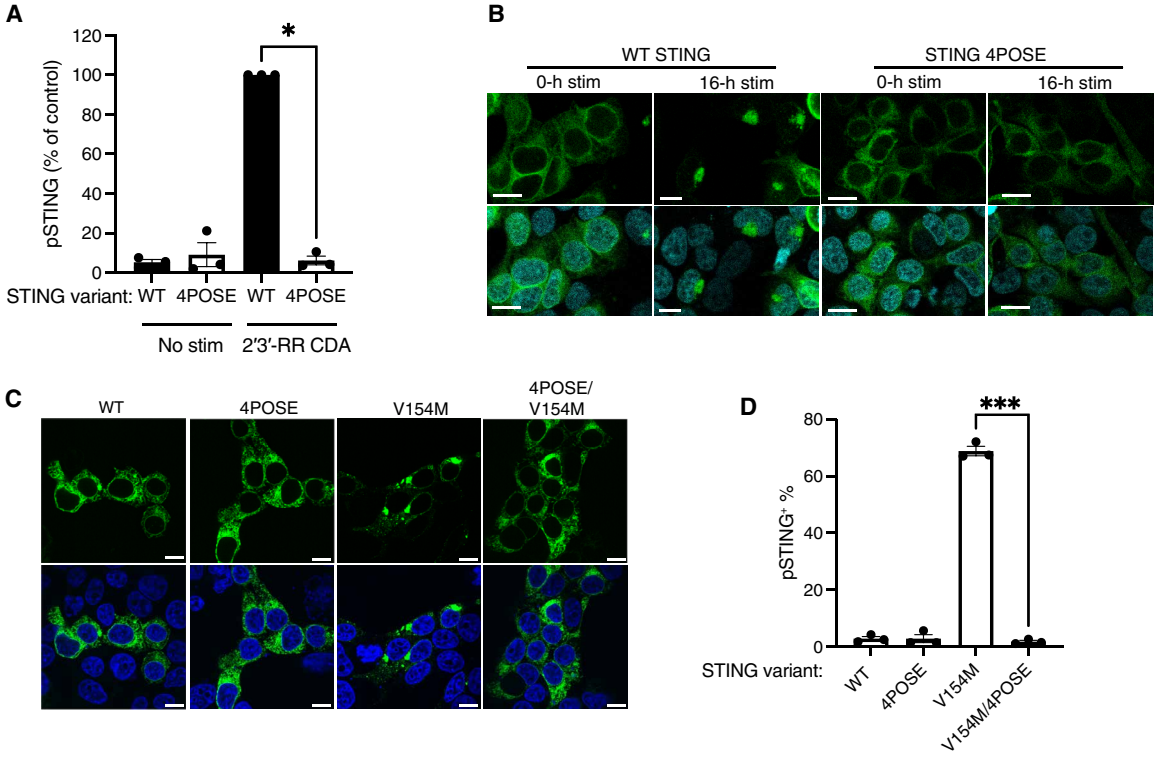

Fig. 6. Mutating the PI4P binding site of STING prevents STING activation. (**A**) STING phosphorylation in 293T cells transfected with WT eGFP-STING or eGFP-STING 4POSE. Cells were stimulated with 2′3′-RR CDA before quantification of STING phosphorylation by flow cytometry. Means ± SEM of $n = 3$ biological replicates of three independent experiments are shown. A one-tailed paired *t* test was performed on non-normalized data for the indicated samples. $^{*}P < 0.05$. (**B**) Microscope images of STING cluster formation in 293T cells transfected with WT eGFP-STING or eGFP-STING 4POSE stimulated for the indicated hours with 2′3′-RR CDA. Scale bars, 10 μm. Nuclei were counterstained using Hoescht. Representative images of $n = 3$ biological replicates of three independent experiments are shown. (**C**) Microscope images of STING cluster formation in 293T cells transfected with the indicated eGFP-STING variants. Scale bars, 10 μm. Nuclei were counterstained using DAPI. Representative images of $n = 3$ biological replicates are shown. (**D**) STING phosphorylation quantified by flow cytometry in 293T cells transfected with indicated STING variants. Means ± SEM of $n = 3$ biological replicates of three independent experiments are shown. A paired one-tailed *t* test was performed to compare the indicated groups. $^{***}P < 0.001$.

transported back to the ER to terminate immune signaling (*40*). The mechanisms regulating trafficking and retention of STING in the Golgi and subsequent egress from the Golgi are not well understood, although a role for adaptor protein complex 1 (AP-1) has been demonstrated in the process (*13*). We showed that the intensity of STING activation and its subsequent degradation depended on proteins that affected PI4P levels at the TGN, including PI4KB, Sac1, OSBP, and ACBD3.

ACBD3 is a multifunctional protein involved in various cellular processes, including recruitment of PI4KB to the TGN (*41*), hormone-induced steroid formation at mitochondria by binding to PKA (*42*), and iron uptake by the divalent metal transporter 1 (DMT1) (*43*). Because PI4KB was also a hit in our primary screen for STING activation but not any of the other known ACBD3 binding partners, we focused on the role of ACBD3 and PI4KB in STING activation. As reported previously (*44*), we observed that ACBD3 depletion markedly altered the intracellular distribution of PI4KB and PI4P. The role of PI4P in STING activation was established by reducing PI4P production at the TGN either by inhibiting PI4KB or by increasing PI4P hydrolysis by Sac1. Conversely, increasing PI4P abundance by inhibiting the lipid transfer protein OSBP markedly enhanced STING activation. Therefore, we concluded that PI4P levels at the TGN dictate the intensity of the STING-induced immune response. These results were in line with a work showing that hydrolyzing PI4P in the vicinity of STING by Sac1 prevented STING activation (*45*).

How PI4P affects STING activation remains poorly understood. PI4P lipids can anchor various proteins to the Golgi via their PI4P-interacting domains, such as PH domains. Binding is partly driven by electrostatic interactions between the inositol head group of PI4P and cationic residues in PH domains (*46*). Although STING shows no homology to known PI4P-binding domains, the purified C-terminal domain of STING can bind PI4P lipids (*33*). Computational modeling of STING in an active conformation pointed to a patch of basic amino acids in close proximity to the transmembrane helices of STING that can accommodate PI4P (*33*). Our results revealed that changing these basic amino acids to glutamate in the STING 4POSE mutant prevents STING cluster formation and activation, suggesting that STING may directly interact with PI4P at the TGN. Retargeting STING to PI4P-enriched membranes using the PH domain of FAPP1 led to STING activation, even in the absence of a stimulus. A direct interaction between STING and PI4P at PI4P-enriched membranes seems to be required for activation, because the STING 4POSE mutant was not activated despite its relocalization. Besides directly interacting with STING, PI4P may promote STING trafficking by facilitating the general process of ER-to-Golgi transport of proteins. In yeast, for example, coat protein complex II (COP-II) vesicle fusion

Downloaded from https://www.science.org on March 18, 2024

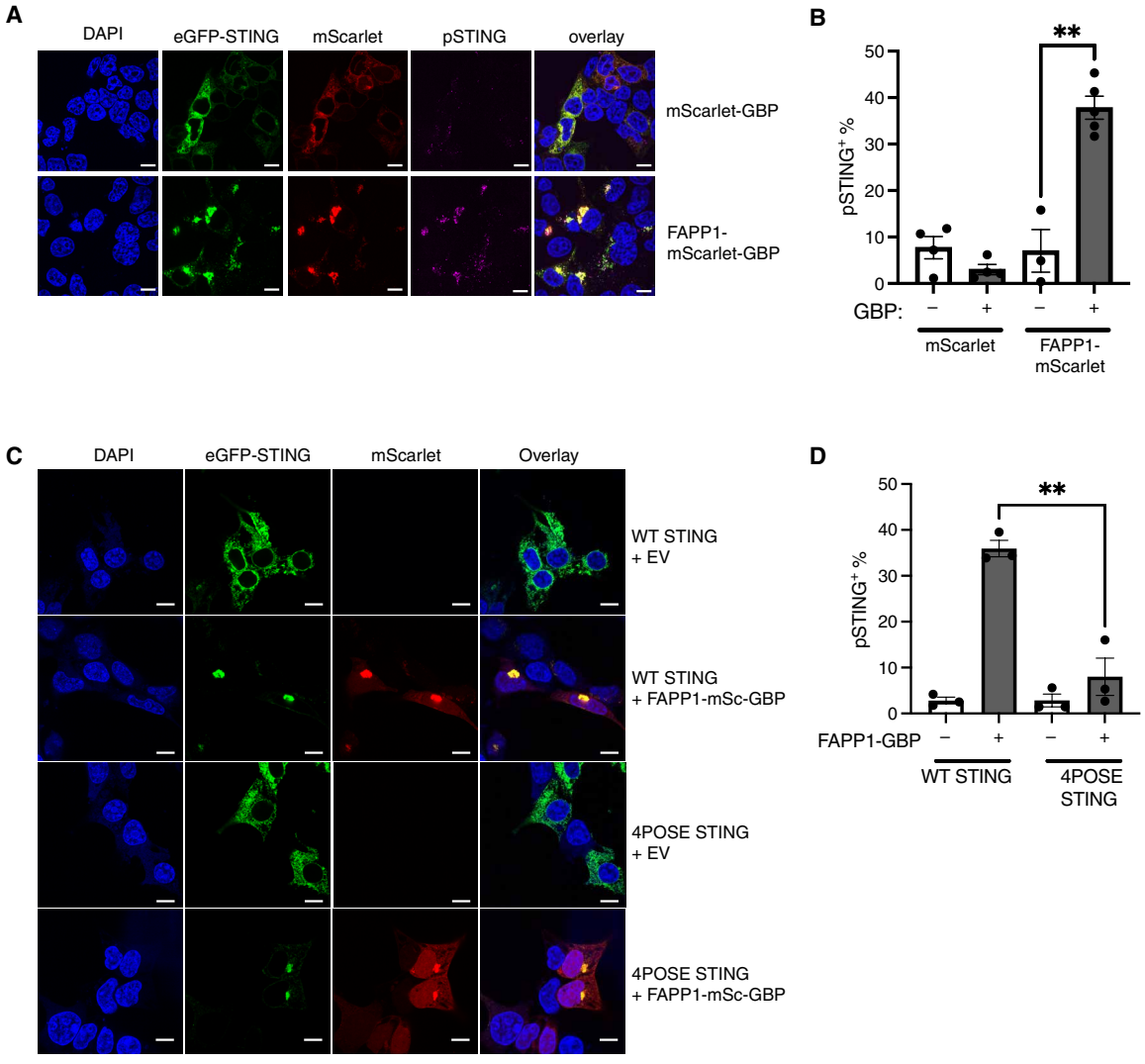

Fig. 7. Targeting STING to PI4P-enriched areas promotes STING activation in the absence of STING agonist. (**A**) Microscope images of 293T cells transfected with eGFP-STING and the indicated mScarlet-GBP fusion constructs. Scale bar, 10 μm. Representative images of $n = 3$ biological replicates of three independent experiments are shown. (**B**) STING phosphorylation in 293T cells transfected with eGFP-STING and mScarlet constructs. After transfection, STING phosphorylation was quantified by flow cytometry. Means ± SEM of $n = 4$ biological replicates of four independent experiments are shown. A paired one-tailed *t* test was performed to compare the indicated groups. $^{**}P < 0.01$. (**C**) Microscope images of 293T cells transfected with WT or 4POSE eGFP-STING and empty vector or FAPP1-mScarlet-GBP constructs. Representative images of $n = 3$ biological replicates of three independent experiments are shown. Scale bar, 10 μm. (**D**) STING phosphorylation in 293T cells transfected with WT or 4POSE eGFP-STING and empty vector or FAPP1-mScarlet (mSc)-GBP constructs. After transfection, STING phosphorylation was quantified by flow cytometry. Means ± SEM of at least $n = 3$ biological replicates of three independent experiments are shown. A paired one-tailed *t* test was performed to compare the indicated groups. $^{**}P < 0.01$.

depends on cis-Golgi–localized PI4P (*47*). In mammalian cells, however, the role of PI4P in COP-II vesicle transport remains to be elucidated.

The impact of ACBD3 on STING activation varied somewhat depending on the STING agonist examined. Specifically, although ACBD3 depletion substantially reduced the response to 2′3′-cGAMP, the impact was less notable than for the other STING agonists tested. This may be due to a slower rate of dissociation of 2′3′-cGAMP from the ligand binding domain of STING compared with the other STING agonists (*48*). A lower dissociation rate may allow STING activation through a single binding event, whereas activation by other STING agonists may require multiple binding events of the ligand and continuous exposure to activating concentrations of the STING agonist (*48*). The responses to STING agonists with faster dissociation rates may be more greatly affected when STING concentrations in the Golgi are limiting because of the absence of ACBD3. In line with this notion, prolonged stimulation or higher ligand concentrations diminishes the effect of ACBD3 on STING activation (*49*).

OSBP shuttles TGN-localized PI4P to the ER in exchange for cholesterol, which moves in the opposite direction. Thus, OSBP inhibition not only increases PI4P at the TGN but also increases cholesterol levels at the ER membrane (*50*). The subcellular distribution of cholesterol may also affect STING activation. For example, STING is constitutively active in cells lacking the lysosomal cholesterol transporter

Downloaded from https://www.science.org on March 18, 2024

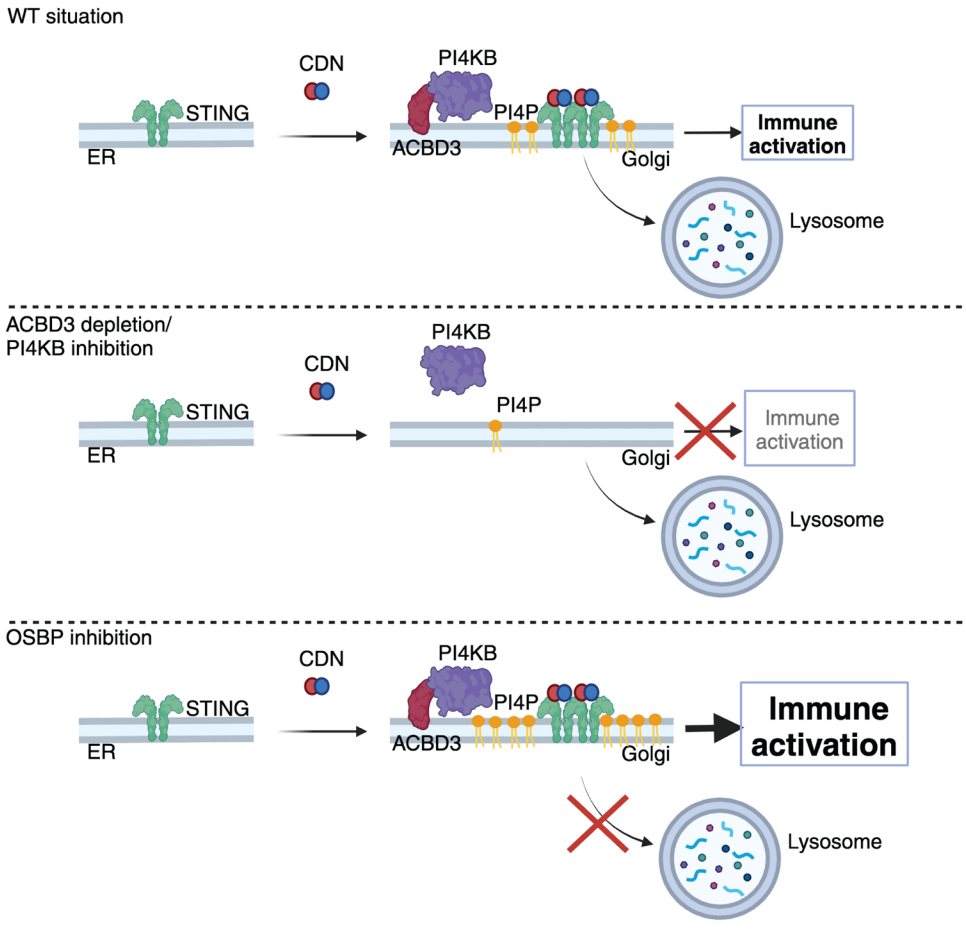

Fig. 8. Model of PI4P-dependent STING activation in the Golgi. In a WT situation, STING moves to PI4P-rich membranes of the Golgi, where it interacts with PI4P and forms activation clusters required for downstream immune signaling. After activation, STING is degraded by the lysosome. Upon ACBD3 depletion or PI4KB inhibition, PI4P levels in the Golgi are reduced and no STING activation clusters are formed, thereby preventing downstream immune activation. Upon OSBP inhibition, PI4P levels in the Golgi are increased and the formation of STING activation clusters is promoted, thereby enhancing downstream immune activation. Created with Biorender.com.

NPC1 because of a reduction in ER-cholesterol (*51*). Similarly, STING was shown to be activated upon a decrease in ER-localized cholesterol in another study (*52*). Although a buildup of cholesterol in the ER resulting from OSBP inhibition might then be predicted to dampen STING activation, our results demonstrated an increase in STING activation after OSBP inhibition. These findings indicated that the accumulation of PI4P is a dominant factor in STING activation. We found that inhibiting PI4P production nullifies the boosting effect of OSBP inhibitors. Our results also suggested that the previously documented increase in STING activation upon ER-cholesterol depletion may be caused by PI4P accumulation at the TGN, because ER-cholesterol depletion prevents PI4P shuttling by OSBP and thus has a similar effect as OSBP inhibition (*29*).

Itraconazole is an established antifungal and is being evaluated as an anticancer drug (*53*). Apart from OSBP (*30*), itraconazole has several targets, including the Hedgehog pathway (*54*), vascular endothelial growth factor receptor 2 (*55*), voltage-dependent anion-selective channel 1 (VDAC1) (*56*) and Niemann-Pick disease, type C1 (NPC1) (*57*). Knockout of the lysosomal protein NPC1 results in tonic STING activation because of the depletion of ER cholesterol, which causes relocation of the cholesterol sensor SREBP2 and STING to the Golgi, and by preventing lysosomal degradation of STING, thereby boosting immune activation (*51*). NPC1 deficiency also results in PI4P accumulation at the TGN and may promote STING activation as a result, in accord with our findings (*58*). Itraconazole may boost STING responses in part by inhibiting NPC1. Although we did not observe STING activation in the absence of NPC1 in itraconazole-treated cells, inhibition of NPC1 may partially explain the boosting effect of itraconazole. In contrast, the structurally unrelated OSBP-inhibitor OSW-1 is highly specific for OSBP and interacts with OSBP in the nanomolar range via a binding site that is different from itraconazole (*59*). OSW-1 is not known to inhibit NPC1 or any other target of itraconazole. Thus, the major effect of OSW-1 or itraconazole on STING activation is likely via OSBP inhibition. Supporting this notion, NPC1, SREBP2, or other cholesterol-regulating factors were not identified as hits in our genome-wide screens for STING regulators (*21*).

Enhancing STING activation by itraconazole or other OSBP inhibitors has therapeutic potential by promoting the immune response to virus-infected or cancer cells. In cancer cells, accumulation of cytosolic DNA can activate the cGAS/STING pathway and promote tumor clearance, although some cancer cells epigenetically silence STING or express STING mutants with reduced activity (*60*). In these cases, increasing Golgi PI4P levels (e.g., via OSBP inhibition) may improve the endogenous STING response. Furthermore, treatment of tumors with DNA damaging agents (*61*) or irradiation (*62*, *63*) can provoke STING activation, which may be enhanced upon OSBP inhibition. OSBP inhibitors may also improve the antitumor effects of STING agonists used therapeutically. In line with this proposal, intratumoral injection of cGAMP in combination with bafilomycin A1,

Downloaded from https://www.science.org on March 18, 2024

which prevented lysosomal degradation of STING, markedly improved tumor cell clearance in vivo (*32*). STING is also frequently targeted by viruses in infected cells, thereby dampening the innate immune response (*64*). In that instance, inadequate STING activation may also be restored by treatment with itraconazole or other OSBP inhibitors.

In conclusion, in this study, we demonstrated that STING activation is controlled by PI4P, and we provide mechanistic insights into the important role of this phospholipid in STING-mediated immune activation. Targeting this pathway by (repurposed) drugs may open new avenues for therapies that depend on STING activation.

MATERIALS AND METHODS

Cell lines

All cell lines were cultured at 37°C in humidified atmosphere containing 5% CO_2 with medium supplemented with penicillin (100 U ml^{-1}), streptomycin (100 μg ml^{-1}), glutamine (0.2 mg ml^{-1}), gentamycin sulfate (10 μg ml^{-1}), 20 mM Hepes, 45 μM 2-mercaptoethanol, and 10% heat-inactivated fetal calf serum. Human monocytic THP-1 cells were cultured in RPMI medium, and human embryonic kidney 293T (293T) cells and 293T transfected with human STING (293T + hSTING) were cultured in Dulbecco's modified Eagle's medium (DMEM) medium. THP-1 and 293T cells were from existing stocks in the laboratory. The 293T + hSTING cells were generated as described previously (*14*). Cells were routinely tested for mycoplasma.

Antibodies and reagents

The following antibodies were obtained from Cell Signaling Technology: rabbit–anti-human TBK1 monoclonal (clone D1B4; 1:500 for immunoblot), rabbit–anti-human p-TBK1 monoclonal (clone D52C2; 1:1000 for immunoblot), rabbit–anti-human STING monoclonal (clone D2P2F; 1:2000 for immunoblot), rabbit–anti-human p-STING monoclonal (clone D7C3S; 1:1000 for immunoblot and 1:800 for flow cytometry), rabbit–anti-human p-IRF3 monoclonal (clone 4D4G, 1:1000 for immunoblot), and rabbit–anti-IκBalpha (clone 9242S; used 1:500 for immunoblot). Antibodies obtained from LI-COR Biosciences were as follows: goat–anti-mouse IgG IRDye 680RD conjugated (catalog no. 926-68070; used at 1:5000), donkey–anti-rabbit IgG IRDye 800CW conjugated (catalog no. 926-32213; used at 1:5000), and donkey–anti-rabbit IgG IRDye 680RD (catalog no. 926-68073; used at 1:5000). Other antibodies used were as follows: rabbit–anti-human IRF3 monoclonal (Abcam, catalog no. EP2419Y; 1:2000 for immunoblot), mouse–anti-human transferrin receptor monoclonal (Thermo Fischer Scientific, clone H68.4; 1:1000 for immunoblot), mouse-anti-actin (Sigma-Aldrich, catalog no. A5441; 1:5000 for immunoblot), rabbit–anti-PI4KB (FineTest, catalog no. FNab06427; 1:100 for immunofluorescence), mouse IgM–anti-PI4P (Echelon Biosciences, Z-P004; 1:100 for immunofluorescence), rabbit–anti-TGN46 (Novus Biologicals, catalog no. NBP1-49643; 1:400 for immunofluorescence), mouse–anti-ACBD3 (Sigma-Aldrich, catalog no. WH0064746M1; 1:100 for immunofluorescence and flow cytometry and 1:1000 for immunoblot), and rat–anti-hemagglutinin (HA) (clone 3F10, Roche catalog no. 11867423001; 1:500 for immunofluorescence). The following secondary antibodies were from Invitrogen: goat–anti-mouse Alexa Fluor 488–conjugated (catalog no. A11001), goat–anti-rat Alexa Fluor 568–conjugated (catalog no. A11011), goat–anti–mouse-IgM Alexa Fluro 568–conjugated (catalog no. A21043), donkey–anti-rabbit Alexa Fluor 647–conjugated (catalog no. A31573), donkey–anti-mouse Alexa Fluor 568–conjugated (catalog no. A10037), and donkey–anti-mouse Alexa Fluor 647–conjugated (catalog no. A10037).

Reagents used include itraconazole (Santa Cruz Biotechnology, catalog no. sc-205724A), OSW-1 (a kind gift from M. Shair, Harvard University), BF738735 (Tocris, catalog no. 6246/10), polybrene (EMD Millipore, catalog no. TR1003G), diABZI (InvivoGen, catalog no. tlrl-diabzi), 3′3′-CDA (InvivoGen, catalog no. tlrl-nacda), 2′3′-RR CDA (2′3′-RR-S2 CDA) (InvivoGen, catalog no. tlrl-nacda2r), 2′3′-cGAMP (InvivoGen, catalog no. tlrl-nacga23), DMXAA (InvivoGen, catalog no. tlrl-dmx), VACV-70 dsDNA (InvivoGen, catalog no. tlrl-vav70n), and human IFN-β (PeproTech, catalog no. 300-02B). Antibiotic selection was carried out with puromycin (at 2 μg ml^{-1}; Sigma-Aldrich, catalog no. P8833), blasticidin (at 10 μg ml^{-1}; InvivoGen, catalog no. ant-bl-1), and zeocin (at 200 μg ml^{-1}; InvivoGen, catalog no. ant-zn-1).

Plasmids and expression

The lentiviral vector encoding the tdTomato reporter gene driven by the ISREs and the minimal mouse IFN-β promoter were generated as described previously (*21*). For rescue and overexpression, *ACBD3* was cloned into a dual promoter lentiviral vector coexpressing the blasticidin resistance gene and the fluorescent gene mAmetrine (*65*). For overexpression of mScarlet, mScarlet-GBP1, or eGFP-coupled to the N terminus of mSTING via a linker sequence (amino acid sequence GAGAKLGTELGS), the (fusion) construct was generated as gBlock (Integrated DNA Technologies) and cloned using Gibson assembly into a dual promoter lentiviral vector coexpressing the blasticidin resistance gene. For CRISPRi-mediated depletions, cells were transduced with a lentiviral dCas9-HA-BFP-KRAB-NLS expression vector (Addgene, plasmid no.102244).

For gene depletions using individual CRISPRi gRNAs, top enriched gRNAs (table S1) from the screen for STING activation were cloned into the same expression plasmid used for the gRNA library (pCRISPRia-v2, Addgene, plasmid no. 84832, a gift from J. Weissman). The lentiviral gRNA plasmid coexpressed a puromycin resistance gene and blue fluorescence protein (BFP) via a T2A ribosomal skipping sequence controlled by the human EF1A promoter. Conventional CRISPR gRNAs (see table S1) were cloned into a puromycin-selectable lentiviral CRISPR-Cas9 vector, as described previously (*66*). *Sac1* WT [a generous gift from P. Mayinger (OHSU)], the catalytically inactive C389S mutant, or the Golgi-directed K583A K585A double mutant (KKAA) was fused to the N terminus of the fluorescent gene mTurquoise2 via a linker sequence (encoding MTSKSGGGGSGGGG) and cloned using NEBuilder Hifi DNA assembly (New England Biolabs) into a dual promoter lentiviral vector coexpressing a puromycin resistance gene. A plasmid encoding the FAPP1-PH domain (residues 1 to 101) fused to GFP via a linker sequence (DPPVAT) [a generous gift from T. Balla (NIH/NICHD)] was used as template to generate the FAPP1-PH mScarlet-GBP and FAPP1-PH-mScarlet constructs via Gibson assembly into a dual promoter lentiviral vector coexpressing the puromycin resistance gene. Plasmids were transiently transfected into cells using Lipofectamine 2000 (Invitrogen) or stably transduced upon lentivirus production (as indicated in the legends). Lentivirus was produced by transfecting lentiviral plasmids and second generation packaging and polymerase plasmids into 293T cells, as described previously (*21*).

Downloaded from https://www.science.org on March 18, 2024

CDN and IFN-β stimulation reporter assays

Stimulation with CDNs or IFN-β was performed as described previously (*21*). Briefly, the day before stimulation, cells were seeded to 0.5×10^6 cells per ml. Cells were stimulated with CDNs (2′3′-RR CDA: 2 μg ml^{-1} as anonlimiting concentration and 0.5 μg ml^{-1} as a limiting concentration; 2′3′-cGAMP: 20 μg ml^{-1} as a nonlimiting concentration and 7 μg ml^{-1} as a limiting concentration; 3′3′-CDA 40 μg ml^{-1}; 3′3′-cGAMP: 40 μg ml^{-1}; diABZI: 40 ng ml^{-1}) or IFN-β (100 ng ml^{-1}) in 96-well plates using 30,000 cells per well in 150 μl of medium. After 18 to 24 hours, cells were transferred to a 96-well plate, and tdTomato expression was measured by flow cytometry using a high-throughput plate reader on a BD LSR Fortessa or a Beckman Coulter Cytoflex. For stimulations in the presence of itraconazole (10 μM), OSW-1 (10 nM), and/or BF738735 (10 μM), cells were incubated with compounds or DMSO as vehicle 1 hour before stimulations with CDNs or IFN- β. At 18 to 24 hours after stimulation, tdTomato reporter expression was quantified by flow cytometry using a high-throughput plate reader on a BD LSR Fortessa or a Beckman a Beckman Coulter Cytoflex.

IFN-β ELISA

THP-1 cells were seeded to 0.5×10^6 cells in 250 μl. Cells were incubated for in the presence of DMSO or itraconazole (10 μM). After 1 hour, 2′3′-cGAMP (20 μg ml^{-1}) was added, and cells were incubated for 20 to 22 hours. Supernatant was harvested, and IFN-β concentrations were measured using the human IFN-β Quantikine ELISA Kit (R&D Systems, catalog no. DIFNB0) according to the manufacturer's recommendations. Absorbance was measured using a Fluostar Omega microplate reader (BMG Labtech).

Production of *ACBD3* knockout cell lines

As an alternative approach to corroborate the role of *ACBD3* in CDN responses, *ACBD3* was targeted in THP-1 or 293T cells using the conventional CRISPR-Cas9 system. THP-1 cells were transduced, and 293T cells were transfected with a CRISPR-Cas9 lentiviral plasmid encoding a control gRNA or a gRNA targeting *ACBD3* (see table S1). After transduction/transfection, cells were selected using puromycin for 2 days and single-cell cloned by limited dilution (100 cells diluted in 50 ml and plated on 96-well plates using 200 μl per well). Control cells and *ACBD3*-targeted cells were selected that had comparable forward and side scatter by flow cytometry analysis, and *ACBD3* knockout cells were screened by measuring intracellular ACBD3 expression by flow cytometry.

CDN uptake

The production and uptake of [^{32}P]2′3′-cGAMP and [^{32}P]3′3′-CDA were performed as described previously (*21*). For the uptake of 2′3′-cGAMP in cells treated with itraconazole (fig. S5B), cells were pretreated for 1 hour with itraconazole and subsequently stimulated for 8 hours in the presence of 2′3′-cGAMP (20 μg ml^{-1}). After stimulation, cells were washed twice with ice-cold phosphate-buffered saline (PBS), and pellets were lysed in H_2O. 2′3′-cGAMP levels in cell lysates were tested using a 2′3′-cGAMP ELISA kit (Cayman Chemical, catalog no. 501700) according to the manufacturer's recommendations.

Stimulation for reverse transcription–qPCR or immunoblotting

The day before stimulation, cells were seeded to 0.5×10^6 cells per ml. Cells were stimulated with CDNs (2′3′-RR CDA: 5 μg ml^{-1} for nonlimiting concentrations and 1 μg ml^{-1} for limiting concentrations; 2′3′-cGAMP: 20 μg ml^{-1}) or transfected with VACV-70 immunostimulatory DNA (2 μg ml^{-1}) using Lipofectamine 2000 using 0.5×10^6 cells per well in 500 μl of medium. For stimulations in the presence of itraconazole or OSW-1, cells were incubated with compounds or DMSO as vehicle 1 hour before stimulations After stimulations, cells were further processed [see reverse transcription quantitative polymerase chain reaction (qPCR) and immunoblotting].

Reverse transcription–qPCR

Cells were collected and washed in ice-cold PBS. Cells were transferred to ribonuclease-free microcentrifuge tubes, and RNA was isolated using the RNeasy Mini Kit (QIAGEN, catalog no. 74104) including a deoxyribonuclease I step (QIAGEN, catalog no. 79254). RNA concentration was measured by NanoDrop (Thermo Fisher Scientific), and 1 μg of RNA was used as input for cDNA synthesis using the iScript cDNA Synthesis Kit (Bio-Rad, catalog no. 1708890) or SuperScript III (Invitrogen, catalog no. 18080) using random hexamers. cDNA was diluted to 20 ng μl^{-1}, and 2.5 μl per reaction was used as input for the qPCR reaction. qPCR reactions were set up using SSOFast EvaGreen Supermix (Bio-Rad, catalog no. 1725200) or Fast SYBR Green master mix (Applied Biosystems, catalog no. 4385612) according to the manufacturer's recommendations using 500 nM of each primer and the following cycling conditions on a Bio-Rad C1000 Thermal Cycler or Roche LightCycler 480 II: 2 min at 98°C, 40 repeats of 2 s at 98°C and 5 s at 55°C. Primers used to amplify the PCR products specific for the human genes *HPRT1*, *YWHAZ*, *IFNB1*, *IL-6*, *CXCL10*, and *PI4KB* are listed in table S2. The housekeeping genes *HPRT1* and *YWHAZ* served as endogenous controls for cDNA samples.

Cell lysis and immunoblotting

For protein detection by immunoblotting, cells were washed with PBS and lysed in radioimmunoprecipitation assay buffer [25 mM tris-HCl (pH 7.5), 150 mM NaCl, 1 mM EDTA, 1% NP-40, and 0.1% SDS] including cOmplete ULTRA protease inhibitors (Sigma-Aldrich, catalog no. 05892791001), phosphatase inhibitors (Biomake, catalog no. B15001), and 50 mM dithiothreitol. Cell lysates were mixed with 4× NuPAGE LDS sample buffer (Invitrogen, catalog no. NP0007), pulse sonicated, and incubated at 75°C for 5 min. Lysates were loaded onto Bolt 4 to 12% Bis-Tris Plus SDS–polyacrylamide gel electrophoresis (SDS-PAGE) gels (Invitrogen, catalog no. NW04125BOX). Proteins separated by SDS-PAGE were transferred onto Immobilon-FL polyvinylidene difluoride membranes (EMD Millipore) at 100 V for 1 hour at 4°C. Membranes were blocked in 4% nonfat milk (NFM) and probed in 1% NFM overnight at 4°C with primary antibody. Membranes were subsequently washed three times in 1× tris-buffered saline (TBS) including Tween 20 (0.05%) (TBS-T) and probed with secondary antibody for 1 hour at room temperature while protected from light. Membranes were washed two times in TBS-T and once in TBS, and blots were imaged using an Odyssey CLx System (LI-COR).

Intracellular phospho-STING stainings upon transfection

293T cells were transfected with plasmids indicated in the legends. Twenty-four hours after transfection, cells were stimulated for 8 hours with 2′3′-RR CDA (10 μg ml^{-1}). After stimulation, cells were washed and blocked using TruStain Fc receptor blocking solution (BioLegend, catalog no. 422302) for 10 min at RT. Cells were fixed

Downloaded from https://www.science.org on March 18, 2024

in 2% formaldehyde in PBS for 10 min at 4°C. Cells were permeabilized in Perm/Wash buffer (BD Biosciences, catalog no. 554714) for 15 min at 4°C. Cells were incubated with primary antibody in Perm/Wash buffer for 30 min at 4°C, washed, and incubated in secondary antibody for 30 min at 4°C. Cells were washed and analyzed by flow cytometry (Beckman Coulter Cytoflex).

Confocal microscopy

The day before seeding onto microscopy slides, cells were seeded to 0.5×10^6 cells per ml. For live-cell imaging, 293T cells were reseeded onto a Ibidi four-well chambers (Ibidi, catalog no. 80416) treated the day before with fibronectin (5 μg ml^{-1}; Sigma-Aldrich, catalog no. F1141). Cells were allowed to recover for 2 days and used for live cell imaging in a humidified temperature and CO_2-controlled chamber using a Nikon A1R confocal microscope. For fixed-sample confocal microscopy, 293T or THP-1 cells were reseeded onto an Ibidi μ-Slide 18-well (catalog no. 81826) treated the day before with fibronectin (5 μg ml^{-1}). 293T cells were allowed to recover for 2 days before stimulation and staining. Before stimulation and staining of THP-1 cells, cells were treated overnight with phorbol 12-myristate 13-acetate (PMA) (30 ng ml^{-1}; Sigma Aldrich catalog no. P1585) followed by overnight recovery in PMA-free medium. Cells were stimulated with CDNs (2'3'-RR CDA 10 μg ml^{-1}; 2'3'-GAMP: 20 μg ml^{-1}) for the indicated time points and fixed using 2% formaldehyde for 15 min at RT. Samples were incubated with 50 mM NH_4Cl in PBS for 10 min at RT and permeabilized with 0.2% Triton X-100 in PBS for 15 min at RT. Samples were blocked in 3% bovine serum albumin (BSA) and 0.2% Triton X-100 in PBS for 45 min at RT. Cells were washed incubated with indicated primary antibodies for 1 hour at RT, washed, and incubated in secondary antibodies for 1 hour at RT in 0.3% BSA and 0.02% Triton X-100. Cells were washed and kept in PBS + 4′,6-diamidino-2-phenylindole (DAPI) at 4°C until imaging on a Nikon A1R confocal microcope. For PI4P staining, after fixing, cells were permeabilized with 20 μM digitonin in buffer A [20 mM Pipes (pH 6.8), 137 mM NaCl, and 2.7 mM KCl]. Cells were blocked using 5% normal goat serum (NGS) and 50 mM NH_4Cl in buffer A for 45 min at RT. Cells were incubated in primary antibodies in buffer A supplemented with 5% NGS for 1 hour at RT, washed, and incubated in secondary antibodies in buffer A supplemented with 5% NGS for 1 hour at RT. Cells were incubated in 2% formaldehyde for 10 min at RT, washed, and kept in PBS + DAPI at 4°C until imaging on a Nikon A1R confocal microscope or Olympus IX SpinSR confocal microscope. Images were processed and eGFP-positive clusters were counted using Fiji.

Statistical analysis

Statistical analyses were performed using Graphpad Prism (version 10.0). Data are presented as means ± SEM of at least three biological replicates (as indicated in the figure legends). For normalized (qPCR) data performed multiple times, one-sample *t* tests were performed to compare treatment groups with a control value (usually 100; see legends). To compare multiple treatment groups with a control group using the data that were not normalized to a control value (as indicated in the legends), we performed one-way analysis of variance (ANOVA) followed by Dunnett's multiple comparison tests of each treatment group with the control group. To compare two treatment groups with data that passed normality tests, we performed paired or unpaired (depending on the circumstances) one-tailed *t* tests. To compare multiple treatment groups over time, we performed two-way ANOVA tests followed by Tukey's multiple comparisons post tests.

Supplementary Materials

This PDF file includes:
Figs. S1 to S7
Tables S1 and S2

Other Supplementary Material for this manuscript includes the following:
MDAR Reproducibility Checklist

REFERENCES AND NOTES

1. H. Ishikawa, G. N. Barber, STING is an endoplasmic reticulum adaptor that facilitates innate immune signalling. *Nature* **455**, 674–678 (2008).
2. R. J. Dey, B. Dey, Y. Zheng, L. S. Cheung, J. Zhou, D. Sayre, P. Kumar, H. Guo, G. Lamichhane, H. O. Sintim, W. R. Bishai, Inhibition of innate immune cytosolic surveillance by an M. tuberculosis phosphodiesterase. *Nat. Chem. Biol.* **13**, 210–217 (2017).
3. J. J. Woodward, A. T. Lavarone, D. A. Portnoy, c-di-AMP secreted by intracellular Listeria monocytogenes activates a host type I interferon response. *Science* **328**, 1703–1705 (2010).
4. J. R. Barker, B. J. Koestler, V. K. Carpenter, D. L. Burdette, C. M. Waters, R. E. Vance, R. H. Valdivia, STING-dependent recognition of cyclic di-AMP mediates type I interferon responses during chlamydia trachomatis infection. *mBio* **4**, e00018-13 (2013).
5. J. Ahn, D. Gutman, S. Saijo, G. N. Barber, STING manifests self DNA-dependent inflammatory disease. *Proc. Natl. Acad. Sci. U.S.A.* **109**, 19386–19391 (2012).
6. A. Gall, P. Treuting, K. B. Elkon, Y.-M. Loo, M. Gale Jr., G. N. Barber, D. B. Stetson, Autoimmunity initiates in nonhematopoietic cells and progresses via lymphocytes in an interferon-dependent autoimmune disease. *Immunity* **36**, 120–131 (2012).
7. S.-R. Woo, M. B. Fuertes, L. Corrales, S. Spranger, M. J. Furdyna, M. Y. K. Leung, R. Duggan, Y. Wang, G. N. Barber, K. A. Fitzgerald, M.-L. Alegre, T. F. Gajewski, STING-dependent cytosolic DNA sensing mediates innate immune recognition of immunogenic tumors. *Immunity* **41**, 830–842 (2014).
8. A. R. Lam, N. Le Bert, S. S. Ho, Y. J. Shen, L. F. Tang, G. M. Xiong, J. L. Croxford, C. X. Koo, K. J. Ishii, S. Akira, D. H. Raulet, S. Gasser, RAE1 ligands for the NKG2D receptor are regulated by STING-dependent DNA sensor pathways in lymphoma. *Cancer Res.* **74**, 2193–2203 (2014).
9. A. M. Green, P. R. Beatty, A. Hadjilaou, E. Harris, Innate immunity to dengue virus infection and subversion of antiviral responses. *J. Mol. Biol.* **426**, 1148–1160 (2014).
10. C. K. Holm, S. H. Rahbek, H. H. Gad, R. O. Bak, M. R. Jakobsen, Z. Jiang, A. L. Hansen, S. K. Jensen, C. Sun, M. K. Thomsen, A. Laustsen, C. G. Nielsen, K. Severinsen, Y. Xiong, D. L. Burdette, V. Hornung, R. J. Lebbink, M. Duch, K. A. Fitzgerald, S. Bahrami, J. G. Mikkelsen, R. Hartmann, S. R. Paludan, Influenza A virus targets a cGAS-independent STING pathway that controls enveloped RNA viruses. *Nat. Commun.* **7**, 10680 (2016).
11. K. Maringer, A. Fernandez-Sesma, Message in a bottle: Lessons learned from antagonism of STING signalling during RNA virus infection. *Cytokine Growth Factor Rev.* **25**, 669–679 (2014).
12. S. Aguirre, A. Fernandez-Sesma, Collateral Damage during Dengue Virus Infection: Making Sense of DNA by cGAS. *J. Virol.* **91**, e01081-16 (2017).
13. A. Ablasser, S. Hur, Regulation of cGAS- and RLR-mediated immunity to nucleic acids. *Nat. Immunol.* **21**, 17–29 (2020).
14. L. Corrales, L. H. Glickman, S. M. McWhirter, D. B. Kanne, K. E. Sivick, G. E. Katibah, S. R. Woo, E. Lemmens, T. Banda, J. J. Leong, K. Metchette, T. W. Dubensky Jr., T. F. Gajewski, Direct Activation of STING in the Tumor Microenvironment Leads to Potent and Systemic Tumor Regression and Immunity. *Cell Rep.* **11**, 1018–1030 (2015).
15. B.-C. Zhang, R. Nandakumar, L. S. Reinert, J. Huang, A. Laustsen, Z.-L. Gao, C.-L. Sun, S. B. Jensen, A. Troldborg, S. Assil, M. F. Berthelsen, C. Scavenius, Y. Zhang, S. J. Windross, D. Olagnier, T. Prabakaran, C. Bodda, R. Narita, Y. Cai, C.-G. Zhang, H. Stenmark, C. M. Doucet, T. Noda, Z. Guo, R. Goldbach-Mansky, R. Hartmann, Z. J. Chen, J. J. Enghild, R. O. Bak, M. K. Thomsen, S. R. Paludan, STEEP mediates STING ER exit and activation of signaling. *Nat. Immunol.* **21**, 868–879 (2020).
16. R. Dhanwani, M. Takahashi, S. Sharma, Cytosolic sensing of immuno-stimulatory DNA, the enemy within. *Curr. Opin. Immunol.* **50**, 82–87 (2018).
17. K. W. Ng, E. A. Marshall, J. C. Bell, W. L. Lam, cGAS–STING and cancer: Dichotomous roles in tumor immunity and development. *Trends Immunol.* **39**, 44–54 (2018).
18. J. B. Eaglesham, P. J. Kranzusch, Conserved strategies for pathogen evasion of cGAS–STING immunity. *Curr. Opin. Immunol.* **66**, 27–34 (2020).
19. M. Stempel, B. Chan, V. J. Lisnić, A. Krmpotić, J. Hartung, S. R. Paludan, N. Füllbrunn, N. A. Lemmermann, M. M. Brinkmann, The herpesviral antagonist m152 reveals differential activation of STING-dependent IRF and NF-κB signaling and STING's dual role during MCMV infection. *EMBO J.* **38**, e100983 (2019).
20. J. K. Won, S. F. Bakhoum, The cytosolic dna-sensing cGAS-STING pathway in cancer. *Cancer Discov.* **10**, 26–39 (2020).
21. R. D. Luteijn, S. A. Zaver, B. G. Gowen, S. K. Wyman, N. E. Garelis, L. Onia, S. M. McWhirter, G. E. Katibah, J. E. Corn, J. J. Woodward, D. H. Raulet, SLC19A1 transports immunoreactive cyclic dinucleotides. *Nature* **573**, 434–438 (2019).

Downloaded from https://www.science.org on March 18, 2024

22. X. Yue, Y. Qian, B. Gim, Acyl-CoA-binding domain-containing 3 (ACBD3; PAP7; GCP60): A multi-functional membrane domain organizer. *Int. J. Mol. Sci.* **3**, 2028 (2019).
23. E. J. Dickson, B. Hille, Understanding phosphoinositides: Rare, dynamic, and essential membrane phospholipids. *Biochem. J.* **476**, 1–23 (2019).
24. K. Mukai, H. Konno, T. Akiba, T. Uemura, S. Waguri, T. Kobayashi, G. N. Barber, H. Arai, T. Taguchi, Activation of STING requires palmitoylation at the Golgi. *Nat. Commun.* **7**, 11932 (2016).
25. X. Yue, Y. Qian, B. Gim, I. Lee, Acyl-CoA-Binding Domain-Containing 3 (ACBD3; PAP7; GCP60): A multi-functional membrane domain organizer. *Int. J. Mol. Sci.* **20**, 2028 (2019).
26. H. M. Van Der Schaar, P. Leyssen, H. J. Thibaut, A. de Palma, L. van der Linden, K. H. W. Lanke, C. Lacroix, E. Verbeken, K. Conrath, A. M. Macleod, D. R. Mitchell, N. J. Palmer, H. van de Poël, M. Andrews, J. Neyts, F. J. M. van Kuppeveld, A novel, broad-spectrum inhibitor of enterovirus replication that targets host cell factor phosphatidylinositol 4-kinase IIIβ. *Antimicrob. Agents Chemother.* **57**, 4971–4981 (2013).
27. A. Blagoveshchenskaya, F. Y. Cheong, H. M. Rohde, G. Glover, A. Knödler, T. Nicolson, G. Boehmelt, P. Mayinger, Integration of Golgi trafficking and growth factor signaling by the lipid phosphatase SAC1. *J. Cell Biol.* **180**, 803–812 (2008).
28. F. Nakatsu, A. Kawasaki, Functions of Oxysterol-Binding Proteins at Membrane Contact Sites and Their Control by Phosphoinositide Metabolism. *Front. Cell Dev. Biol.* **9**, 664788 (2021).
29. B. Mesmin, J. Bigay, J. Polidori, D. Jamecna, S. Lacas-Gervais, B. Antonny, Sterol transfer, PI4P consumption, and control of membrane lipid order by endogenous OSBP. *EMBO J.* **36**, 3156–3174 (2017).
30. J. R. P. M. Strating, L. van der Linden, L. Albulescu, J. Bigay, M. Arita, L. Delang, P. Leyssen, H. M. van der Schaar, K. H. W. Lanke, H. J. Thibaut, R. Ulferts, G. Drin, N. Schlinck, R. W. Wubbolts, N. Sever, S. A. Head, J. O. Liu, P. A. Beachy, M. A. De Matteis, M. D. Shair, V. M. Olkkonen, J. Neyts, F. J. M. van Kuppeveld, Itraconazole inhibits enterovirus replication by targeting the oxysterol-binding protein. *Cell Rep.* **10**, 600–615 (2015).
31. S. Amini-Bavil-Olyaee, Y. J. Choi, J. H. Lee, M. Shi, I.-C. Huang, M. Farzan, J. U. Jung, The antiviral effector IFITM3 disrupts intracellular cholesterol homeostasis to block viral entry. *Cell Host Microbe* **13**, 452–464 (2013).
32. V. K. Gonugunta, T. Sakai, V. Pokatayev, K. Yang, J. Wu, N. Dobbs, N. Yan, Trafficking-mediated STING degradation requires sorting to acidified endolysosomes and can be targeted to enhance anti-tumor response. *Cell Rep.* **21**, 3234–3242 (2017).
33. M. Triantafilou, J. Ramanjulu, L. M. Booty, G. Jimenez-Duran, H. Keles, K. Saunders, N. Nevins, E. Koppe, L. K. Modis, G. S. Pesiridis, J. Bertin, K. Triantafilou, Human rhinovirus promotes STING trafficking to replication organelles to promote viral replication. *Nat. Commun.* **13**, 1406 (2022).
34. N. Jeremiah, B. Neven, M. Gentili, I. Callebaut, S. Maschalidi, M.-C. Stolzenberg, N. Goudin, M.-L. Frémond, P. Nitschke, T. J. Molina, S. Blanche, C. Picard, G. I. Rice, Y. J. Crow, N. Manel, A. Fischer, B. Bader-Meunier, F. Rieux-Laucat, Inherited STING-activating mutation underlies a familial inflammatory syndrome with lupus-like manifestations. *J. Clin. Invest.* **124**, 5516–5520 (2014).
35. G. Shang, C. Zhang, Z. J. Chen, X.-C. Bai, X. Zhang, Cryo-EM structures of STING reveal its mechanism of activation by cyclic GMP–AMP. *Nature* **567**, 389–393 (2019).
36. U. Rothbauer, K. Zolghadr, S. Tillib, D. Nowak, L. Schermelleh, A. Gahl, N. Backmann, K. Conrath, S. Muyldermans, M. C. Cardoso, H. Leonhardt, Targeting and tracing antigens in live cells with fluorescent nanobodies. *Nat. Methods* **3**, 887–889 (2006).
37. D. S. Bindels, M. Postma, L. Haarbosch, L. van Weeren, T. W. J. Gadella Jr., Multiparameter screening method for developing optimized red-fluorescent proteins. *Nat. Protoc.* **15**, 450–478 (2020).
38. T. Balla, P. Várnai, Visualization of cellular phosphoinositide pools with GFP-fused protein-domains. *Curr. Protoc. Cell. Biol.*, (2009).
39. H. Kemmoku, Y. Kuchitsu, K. Mukai, T. Taguchi, Specific association of TBK1 with the trans-Golgi network following STING stimulation. *Cell Struct. Funct.* **47**, 19–30 (2022).
40. T. Taguchi, K. Mukai, E. Takaya, R. Shindo, STING Operation at the ER/Golgi Interface. *Front. Immunol.* **12**, 8–13 (2021).
41. J. A. McPhail, J. E. Burke, Drugging the phosphoinositide 3-kinase (PI3K) and phosphatidylinositol 4-kinase (PI4K) family of enzymes for treatment of cancer, immune disorders, and viral/parasitic infections. *Traffic* **24**, 131–145 (2022).
42. J. Liu, H. Li, V. Papadopoulos, PAP7, a PBR/PKA-RIα-associated protein: A new element in the relay of the hormonal induction of steroidogenesis. *J. Steroid Biochem. Mol. Biol.* **85**, 275–283 (2003).
43. Y. Okazaki, Y. Ma, M. Yeh, H. Yin, Z. Li, K. Y. Yeh, J. Glass, DMT1 (IRE) expression in intestinal and erythroid cells is regulated by peripheral benzodiazepine receptor-associated protein 7. *Am. J. Physiol. Gastrointest. Liver Physiol.* **302**, G1180–G1190 (2012).
44. H. Lyoo, H. M. van der Schaar, C. M. Dorobantu, H. H. Rabouw, J. R. P. M. Strating, F. J. M. van Kuppeveld, ACBD3 is an essential Pan-enterovirus host factor that mediates the interaction between Viral 3A protein and cellular protein PI4KB. *mBio* **10**, 1–15 (2019).
45. R. Fang, Q. Jiang, X. Jia, Z. Jiang, ARMH3-mediated recruitment of PI4KB directs Golgi-to-endosome trafficking and activation of the antiviral effector STING. *Immunity* **56**, 500–515.e6 (2023).
46. J. G. Pemberton, T. Balla, Polyphosphoinositide-binding domains: Insights from peripheral membrane and lipid-transfer proteins. *Adv. Exp. Med. Biol.* **1111**, 77–137 (2019).
47. A. Lorente-Rodríguez, C. Barlowe, Requirement for GOLGI-localized PI(4)P in fusion of COPII vesicles with Golgi compartments. *Mol. Biol. Cell* **22**, 216–229 (2011).
48. A. J. Pollock, S. A. Zaver, J. J. Woodward, A STING-based biosensor affords broad cyclic dinucleotide detection within single living eukaryotic cells. *Nat. Commun.* **11**, 1–13 (2020).
49. K. Motani, N. Saito-Tarashima, K. Nishino, S. Yamauchi, N. Minakawa, H. Kosako, The Golgi-resident protein ACBD3 concentrates STING at ER-Golgi contact sites to drive export from the ER. *Cell Rep.* **41**, 111868 (2022).
50. C. Y. Lim, O. B. Davis, H. R. Shin, J. Zhang, C. A. Berdan, X. Jiang, J. L. Counihan, D. S. Ory, D. K. Nomura, R. Zoncu, ER–lysosome contacts enable cholesterol sensing by mTORC1 and drive aberrant growth signalling in Niemann–Pick type C. *Nat. Cell Biol.* **21**, 1206–1218 (2019).
51. T. T. Chu, X. Tu, K. Yang, J. Wu, J. J. Repa, N. Yan, Tonic prime-boost of STING signalling mediates Niemann–Pick disease type C. *Nature* **596**, 570–575 (2021).
52. A. G. York, K. J. Williams, J. P. Argus, Q. D. Zhou, G. Brar, L. Vergnes, E. E. Gray, A. Zhen, N. C. Wu, D. H. Yamada, C. R. Cunningham, E. J. Tarling, M. Q. Wilks, D. Casero, D. H. Gray, A. K. Yu, E. S. Wang, D. G. Brooks, R. Sun, S. G. Kitchen, T. T. Wu, K. Reue, D. B. Stetson, S. J. Bensinger, Limiting cholesterol biosynthetic flux spontaneously engages type I IFN signaling. *Cell* **163**, 1716–1729 (2015).
53. H. Tsubamoto, T. Ueda, K. Inoue, K. Sakata, H. Shibahara, T. Sonoda, Repurposing itraconazole as an anticancer agent. *Oncol. Lett.* **14**, 1240–1246 (2017).
54. J. Kim, J. Y. Tang, R. Gong, J. Kim, J. J. Lee, K. V. Clemons, C. R. Chong, K. S. Chang, M. Fereshteh, D. Gardner, T. Reya, J. O. Liu, E. H. Epstein, D. A. Stevens, P. A. Beachy, Itraconazole, a commonly used antifungal that inhibits hedgehog pathway activity and cancer growth. *Cancer Cell* **17**, 388–399 (2010).
55. B. A. Nacev, P. Grassi, A. Dell, S. M. Haslam, J. O. Liu, The antifungal drug itraconazole inhibits vascular endothelial growth factor receptor 2 (VEGFR2) Glycosylation, Trafficking, and Signaling in endothelial cells. *J. Biol. Chem.* **286**, 44045–44056 (2011).
56. S. A. Head, W. Shi, L. Zhao, K. Gorshkov, K. Pasunooti, Y. Chen, Z. Deng, R. J. Li, J. S. Shim, W. Tan, T. Hartung, J. Zhang, Y. Zhao, M. Colombini, J. O. Liu, Antifungal drug itraconazole targets VDAC1 to modulate the AMPK/mTOR signaling axis in endothelial cells. *Proc. Natl. Acad. Sci. U.S.A.* **112**, E7276–E7285 (2015).
57. M. N. Trinh, F. Lu, X. Li, A. das, Q. Liang, J. K. de Brabander, M. S. Brown, J. L. Goldstein, Triazoles inhibit cholesterol export from lysosomes by binding to NPC1. *Proc. Natl. Acad. Sci. U.S.A.* **114**, 89–94 (2017).
58. C. Kutchukian, O. Vivas, M. Casas, J. G. Jones, S. A. Tiscione, S. Simo, D. S. Ory, R. E. Dixon, E. J. Dickson, *EMBO J.* **40**, e105990 (2021).
59. B. L. Roberts, Z. C. Severance, R. C. Bensen, A. T. le-McClain, C. A. Malinky, E. M. Mettenbrink, J. I. Nuñez, W. J. Reddig, E. L. Blewett, A. W. G. Burgett, Differing activities of oxysterol-binding protein (OSBP) targeting anti-viral compounds. *Antiviral Res.* **170**, 104548 (2019).
60. H. Konno, S. Yamauchi, A. Berglund, R. M. Putney, J. J. Mulé, G. N. Barber, Suppression of STING signaling through epigenetic silencing and missense mutation impedes DNA damage mediated cytokine production. *Oncogene* **37**, 2037–2051 (2018).
61. Z. Wang, J. Chen, J. Hu, H. Zhang, F. Xu, W. He, X. Wang, M. Li, W. Lu, G. Zeng, P. Zhou, P. Huang, S. Chen, W. Li, L. P. Xia, X. Xia, cGAS/STING axis mediates a topoisomerase II inhibitor–induced tumor immunogenicity. *J. Clin. Invest.* **129**, 4850–4862 (2019).
62. L. Deng, H. Liang, M. Xu, X. Yang, B. Burnette, A. Arina, X. D. Li, H. Mauceri, M. Beckett, T. Darga, X. Huang, T. F. Gajewski, Z. J. Chen, Y. X. Fu, R. R. Weichselbaum, STING-dependent cytosolic DNA sensing promotes radiation-induced type I interferon-dependent antitumor immunity in immunogenic tumors. *Immunity* **41**, 843–852 (2014).
63. Q. Storozynsky, M. M. Hitt, The impact of radiation-induced DNA damage on cGAS-STING-mediated immune responses to cancer. *Int. J. Mol. Sci.* **21**, 8877 (2020).
64. T. Hu, M. Pan, Y. Yin, C. Wang, Y. Cui Q. Wang, The regulatory network of cyclic GMP-AMP synthase-stimulator of interferon genes pathway in viral evasion. *Front. Microbiol.* **12**, 1–14 (2021).
65. M. L. van de Weijer, M. C. Bassik, R. D. Luteijn, C. M. Voorburg, M. A. M. Lohuis, E. Kremmer, R. C. Hoeben, E. M. LeProust, S. Chen, H. Hoelen, M. E. Ressing, W. Patena, J. S. Weissman, M. T. McManus, E. J. H. J. Wiertz, R. J. Lebbink, A high-coverage shRNA screen identifies TMEM129 as an E3 ligase involved in ER-associated protein degradation. *Nat. Commun.* **5**, 3832 (2014).
66. F. R. van Diemen, E. M. Kruse, M. J. G. Hooykaas, C. E. Bruggeling, A. C. Schürch, P. M. van Ham, S. M. Imhof, M. Nijhuis, E. J. H. J. Wiertz, R. J. Lebbink, CRISPR/Cas9-mediated genome editing of herpesviruses limits productive and latent infections. *PLOS Pathog.* **12**, e1005701 (2016).

Acknowledgments: We thank E. van t Veld (Centre for Cell Imaging, Faculty of Veterinary Medicine, Utrecht University) and D. Schichnes (the Biological imaging facility, UC Berkeley) for support with the fluorescent microscopy experiments; G. Arkesteijn (Flow Cytometry Facility,

Downloaded from https://www.science.org on March 18, 2024

Faculty of Veterinary Medicine, Utrecht University), H. Nolla, and A. Valeros (Flow Cytometry Facility, UC Berkeley) for technical support with flow cytometry experiments; M. Shair and P. Mayinger for sharing reagents; L. Zhang (UC Berkeley) for laboratory support; Y. Song (UC Berkeley); and the members of the Raulet and van Kuppeveld laboratories for helpful discussions. **Funding:** R.D.L. was supported by the Cancer Research Institute Irvington Postdoctoral Fellowship and a Marie Skłodowska-Curie Individual Fellowship (101030020). The research was supported by grant AI113041 from the US National Institutes of Health to D.H.R. J.J.W. was supported by NIH grant R21-AI137758. S.A.Z. was supported by the University of Washington/Fred Hutchinson Cancer Research Center Viral Pathogenesis Training Program (AI083203), the University of Washington Medical Scientist Training Program (GM007266), and the Seattle ARCS Foundation. **Author contributions:** R.D.L., S.R.v.T., S.A.Z., J.J.W., R.W.W., D.H.R.. and F.J.M.v.K designed the experiments. R.D.L., S.R.v.T., J.E.V.E, L.O., and S.A.Z performed the experiments. R.D.L., D.H.R., and F.J.M.v.K. wrote the manuscript. **Competing interests:** D.H.R. is a cofounder and SAB member of Dragonfly Therapeutics and a member of the SAB of Vivere Pharmaceuticals. **Data and materials availability:** All data needed to evaluate the conclusions in the paper are present in the paper or the Supplementary Materials.

Submitted 11 August 2022
Resubmitted 5 May 2023
Accepted 22 February 2024
Published 12 March 2024
10.1126/scisignal.ade3643

Downloaded from https://www.science.org on March 18, 2024